RESEARCH TECHNICAL REPORT

Fire Plume and Ceiling Layer Correlations and Their Merging

Fire Plume and Ceiling Layer Correlations and Their Merging

Prepared by

Francesco Tamanini

August 2018

FM Global
1151 Boston-Providence Hwy
Norwood, MA 02062

PROJECT ID RW000078

Disclaimer

The research presented in this report, including any findings and conclusions, is for informational purposes only. Any references to specific products, manufacturers, or contractors do not constitute a recommendation, evaluation or endorsement by Factory Mutual Insurance Company (FM Global) of such products, manufacturers or contractors. FM Global does not address life, safety, or health issues. The recipient of this report must make the decision whether to take any action. FM Global undertakes no duty to any party by providing this report or performing the activities on which it is based. FM Global makes no warranty, express or implied, with respect to any product or process referenced in this report. FM Global assumes no liability by or through the use of any information in this report.

Executive Summary

In addition to their importance in describing the characteristics of buoyant flow in thermal plumes and under ceilings, correlations for the evolution of gas temperature and velocity have an important role in practical applications. Those range from the prediction of the response of fire protection devices (smoke detectors, sprinklers, etc.) to the calculation of the convective heat release rate (HRR) from gas temperature measurements in large-scale fire tests. The latter has provided much of the impetus for the work described in the report, which details an evaluation of the consistency of the correlations with concepts of conservation of energy and momentum. In addition, the analysis has described the turning region, where the vertical plume flow merges into the horizontal ceiling layer flow. Ultimately, the improved correlations are implemented in the latest revision of a utility (TarResponse), which is used by FM Global scientists for routine data analysis tasks.

Small adjustments in some of the correlation constants have been derived for the fire plume by enforcing consistency with energy and momentum conservation. The practical impact of these changes, which involve constants that are still within the range of literature values, is relatively modest. Nevertheless, the exercise that has led to their selection is relevant in that it confirms the suitability of the correlations in describing the flow.

In the case of the correlations addressing ceiling layers, one known issue is the approach used to calculate the depth of the ceiling layer. This approach, which has been used up to now, yields unreasonable results for high ceiling clearances. In this case, the problem equations have been critically analyzed using the calculated enthalpy flux as a figure of merit to guide their modification. The changes introduced for the description of the layer depth and of the temperature decay have greatly improved the consistency of the predictions of convective HRR obtained from measurements at different distances from the fire axis. This positive result manifests itself as reduced need to correct the gas temperature measurements to account for heating of the ceiling during long duration tests, with the further benefit that, in most sprinklered fire tests, such correction will not be needed.

The development of a formulation to ensure smooth transition between the fire plume and ceiling layer flows is the last challenge addressed in this work. The transition, which takes place in a turning region near the ceiling, is not covered by the correlations. Though limited in extent, the flow in this region determines first sprinkler activation in the case of under-one conditions. The formulation developed by this analysis is completely empirical. However, it does provide the sought-after smooth transition and it can conceivably be used to estimate the orientation of the velocity vectors in this turning region.

An additional enhancement is currently being developed. It involves accounting for travel time from the fire to the point of measurement, a detail of importance when predicting fire growth rates in rapidly growing fires. In that case, differences in travel time lead to a distorted description of HRR evolution, particularly as the distance of the measurement location from the fire axis increases. Work on this issue is in progress.

Abstract

The report presents a re-evaluation of the correlations used to describe the evolution of gas temperatures and velocities in fire plumes and ceiling layers. The analysis, based on criteria that examine conservation of energy and momentum in the plume and conservation of energy in the layer, has led to the selection of an optimal set of correlations. In addition, the turning region of the flow has been addressed through an empirical formulation, which provides a smooth transition between the vertical flow in the plume and the horizontal flow in the layer. The model based on the modified correlations has been tested against experimental data for pool fires and found to perform satisfactorily. Further improvements to account for flow transit times are in progress and, when implemented, will enhance the capabilities of methods used to extract convective heat release rates and verify sprinkler activations from data for large-scale fire tests.

Acknowledgements

This work has benefited from input and feedback in frequent discussions with several colleagues, particularly those who have been users of the TarResponse utility. The contributions in this area from Kristin Jamison are particularly acknowledged. In addition to providing comments on the utility, Prateep Chatterjee and Karl Meredith have undertaken a review of the manuscript resulting in useful suggestions, most of which have been implemented.

Table of Contents

List of Figures

PAGE LEFT INTENTIONALLY BLANK

1. Introduction and Background

The thermal and flow environment produced by fire plumes as they interact with ceilings largely determines the response of fire detection and protection systems. It is, therefore, not surprising that fire plumes and ceiling layers have been the object of much research interest [1], [2]. The correlations describing the evolution of gas temperature and velocity in these flows have also been used to estimate the convective heat release rate (HRR) and the sprinkler response [3] during fire tests carried out under horizontal flat ceilings. In that work, modifications were introduced to extend the formula for the virtual source of the fire plume to rack-storage arrays more than four tiers high and to correct the anomalous behavior at large ceiling heights of the expression used to calculate the ceiling layer depth. Subsequently, discrepancies among the HRR values obtained from thermocouples at different radial distances from the axis of the fire were resolved by introducing an empirical correlation to account for the gradual heating of the test ceiling in the Large Burn Laboratory (LBL) of the FM Global facility in West Glocester, Rhode Island.

Since ceiling temperature data are the standard input for these analyses, it is important to ensure the reliability of correlations that relate measurements of the thermal environment in the ceiling layer to fire properties of interest, such as the convective HRR. This aspect represents the focus of the first part of the work presented in this report. While there have been many detailed studies of the fire plume and the ceiling layer, much less attention has been paid to the turning region where the two flows merge. However, this area does have some practical relevance, since sprinklers can be located there. A simplified formulation for this transition region is introduced in the second part of this report. Ultimately, all the changes are incorporated into the TarResponse[i] program, which is used for routine analyses of fire test data.

The document considers the following topics. First, it checks the fire plume correlations for compliance with conservation of energy and uses the results of the analysis to guide the selection of the most consistent correlation. Ceiling layer formulations are considered next. They are evaluated using again the evolution of the enthalpy flux to determine their quality. A modified expression for the depth of the ceiling layer is proposed, which corrects some of the inconsistencies revealed by the analysis. The third step addresses the question of the turning region by proposing an empirical formulation that provides a smooth transition of the vertical fire plume flow to the horizontal ceiling layer. Finally, the modified formulation is tested against experimental data from pool fires.

[i] TarResponse is an internally developed utility which calculates sprinkler response and convective HRR for fires carried out under the LBL ceilings, taking as input the temperature measurements from the 125 thermocouples installed under the ceiling. The utility is designed to receive input data in the standardized format used in all tests carried out in the laboratories of the FM Global Research Campus in West Glocester, Rhode Island.

2. Fire Plume Correlations

The characterization of the fire plume is evaluated here by considering the correlations reported in Refs. [1] and [4].

2.1 Temperature Rise

The vertical variation of the centerline temperature in fire plumes, ΔT_0, is given by:

$$\Delta T_0 = 3.5 \cdot T_\infty \qquad \text{and} \qquad \text{2-1}$$

$$\Delta T_0 = 11.0 \cdot T_\infty \left(\frac{R^2}{g\, c_p^2\, p_\infty^2\, M^2} \right)^{1/3} \dot{Q}_c^{2/3} \left(z - z_0 \right)^{-5/3} \quad , \qquad \text{2-2}$$

where the transition from one expression to the other takes place at the height, z_{lim}, at which the temperature rise from the two formulas assumes the same value. That boundary defines the separation between the reacting portion of the fire plume (Eq. 2-1) and its purely buoyant part (Eq. 2-2).

The variables in Eqs. 2-2 and 2-1 are:

- c_p specific heat of gases [= 1000 J/kg K];
- g acceleration of gravity [= 9.806 m/s^2];
- M molecular weight of air [= 29.1 kg/kg-mole];
- p_∞ ambient pressure [= 1.01325·10^5 Pa];
- $\dot{Q}_c$ convective heat release rate [kW];
- R universal gas constant [= 8314 kg m^2/s^2 kg-mole K];
- T_∞ ambient temperature [K];
- z vertical distance [m];
- z_0 elevation of the virtual origin above the fire source [m].

Note that Eq. 2-2 has introduced the virtual origin of the plume, which is calculated from:

$$z_0[m] = z_{0,I}[m] + 0.095 \cdot \dot{Q}_c^{2/5}[kW] \quad , \qquad \text{2-3}$$

$$z_{0,I}[m] = -1.02 \cdot D[m] \qquad \text{for pool fires,} \qquad \text{2-4}$$

$$z_{0,I}[m] = -0.5\left[5 \cdot (n-1) + 4\right] \cdot 0.3048 \qquad \text{for rack storage of } n \text{ tiers,} \qquad \text{2-5}$$

where $z_{0,I}$ is the virtual origin elevation for zero heat release rate. In the above equations, units are indicated when appropriate to account for the fact that numerical values are dimensional. When no units are explicitly provided, the equation is valid regardless of the units used, provided that they are all from a consistent set. This convention has been used throughout the document. Equation 2-5

implements a change introduced subsequent to Ref. [3] to extend the virtual source formula to a number of tiers greater than 4.

By setting the right-hand sides of Eqs. 2-2 and 2-1 equal to each other, and by taking advantage of the equation of state to substitute $\rho_\infty T_\infty$ for $p_\infty M/R$, it is possible to obtain the following expression for the point of transition between the two equations:

$$z_{\lim} - z_0 = \left(\frac{11.0}{3.5}\right)^{3/5} \left(\frac{\dot{Q}_c}{\sqrt{g}\, c_p\, \rho_\infty\, T_\infty}\right)^{2/5} \quad . \qquad 2\text{-}6$$

The height z_{lim} defines the transition between the lower portion of the plume, where chemical reaction is important, and an upper portion, where the fuel has been almost completely depleted and the flow is mostly non-reacting. This view represents a simplified description of the flow compared to that provided by the classic McCaffrey work [5], which identified three regions: continuous flame, intermittent flame, and non-reacting plume. In the first region the temperature is constant, while it decays by the -1 and -5/3 powers of height in the other two. The two transitions among the three regions are defined by values of 0.08 and 0.2 m/kW$^{2/5}$ for the parameter $(z - z_0)/\dot{Q}_c^{2/5}$. As will be introduced later in the simplified form of Eq. 2-6 (see Appendix A), the two-region representation of the fire plume used here puts the transition between the regions at $(z - z_0)/\dot{Q}_c^{2/5}$ = 0.12 m/kW$^{2/5}$.

2.2 Vertical Velocity

The correlation for peak vertical velocity, u_0, in the non-reacting portion of the fire plume is given by Refs. [1, 4] as:

$$u_0 = 4.25 \cdot \left(\frac{g\,R}{c_p\, p_\infty\, M}\right)^{1/3} \dot{Q}_c^{1/3} \left(z - z_0\right)^{-1/3} \quad . \qquad 2\text{-}7$$

Equations 2-2 and 2-7 can be combined to yield the following invariant ratio:

$$u_0 \Big/ \sqrt{2g\left(z - z_0\right)\Delta T_0 / T_\infty} = \frac{4.25}{\sqrt{2 \cdot 11.0}} = 0.906 \quad . \qquad 2\text{-}8$$

Equation 2-7 applies to the plume region for $z > z_{lim}$. At the lower boundary of this region ($z = z_{lim}$), the velocity assumes the value given by:

$$u_{0,\lim} = 4.25 \cdot \left(\frac{3.5}{11.0}\right)^{1/5} \left(\frac{g^2\, R}{c_p\, p_\infty\, M}\right)^{1/5} \dot{Q}_c^{1/5} \quad . \qquad 2\text{-}9$$

The relationship for the velocity in the flame region ($z < z_{lim}$) can be obtained by setting $\Delta T_0/T_\infty = 3.5$ in Eq. 2-8, resulting in:

$$u_0 = 4.25 \cdot \sqrt{\frac{3.5}{11.0}} \sqrt{g\left(z - z_0\right)} \quad . \tag{2-10}$$

It should be noted that the same expression could be written as:

$$u_0 = u_{0,\lim} \sqrt{\frac{z - z_0}{z_{\lim} - z_0}} \quad . \tag{2-11}$$

Similar to what was discussed in connection with the excess temperature profiles, the three regions identified by Ref. [5] are now reduced to two. So, instead of a continuous flame, where the velocity increases as the 1/2 power of height, an intermittent flame with constant velocity and a non-reacting plume with velocity decaying as the -1/3 power of height, the flow is assumed to have only the first and last region.

2.3 Plume Half Width

The plume half width, defined as the radius at which the physical property of interest is equal to half of the centerline value, is given by [1, 4]:

$$b = 0.108 \cdot \left(\frac{T_0}{T_\infty}\right)^{1/2} \left(z - z_0\right) \quad . \tag{2-12}$$

There is some question whether the quantity given by the above equation should apply to the velocity or the temperature profile. In the following discussion, it will be assumed that it is the former (i.e., $b_U = b$) and that the half width (b_T) of the temperature profile is some fraction, α, of b_U:

$$b_T = \alpha b_U \quad , \tag{2-13}$$

where $\alpha = 0.92$ [6].

The radial variation of temperature and vertical velocity in the fire plume will be assumed to be Gaussian, namely:

$$\Delta T = \Delta T_0 \exp(-0.6931 \ (r / b_T)^2) \quad , \tag{2-14}$$

and

$$u = u_0 \exp(-0.6931 \ (r / b_U)^2) \quad , \tag{2-15}$$

where the constant 0.6931 is the numeric value of $\log_e(0.5)$.

It should be noted that the work in Ref. [6] recommended that the profiles for the radial variation of vertical velocity and temperature rise above ambient be approximated as:

$$\frac{\Delta T}{\Delta T_0} = \frac{u}{u_0} = \exp\left(-59\left(r/\left(z-z_0\right)\right)^2\right) \quad . \tag{2-16}$$

When Eqs. 2-15 and 2-16 are set equal to each other and solved for b ($=b_U=b_T$), the expression given as Eq. 2-12 (with $T_0 \cong T_\infty$) is nicely recovered. This result suggests that Eq. 2-12 is generally consistent with the data in Ref. [6] in the limit of small temperature rises.

2.4 Enthalpy Flux

We now consider the implications of the above correlations on the enthalpy flux in the fire plume. This quantity is defined as:

$$\dot{Q}_{ent} = 2\pi \int_0^\infty c_p \, \Delta T \, \rho u \, r \, dr \quad , \tag{2-17}$$

or, by use of the equation of state,

$$\dot{Q}_{ent} = 2\pi \, \rho_\infty \, T_\infty \, c_p \int_0^\infty \frac{\Delta T}{T} u \, r \, dr \quad . \tag{2-18}$$

The internal consistency of the correlations presented above for temperature rise and vertical velocity can be verified by substituting them in Eq. 2-18. After some algebraic manipulation, the expression for the enthalpy flux implied by the correlations for the non-reacting portion of the fire plume becomes:

$$\dot{Q}_{ent} = 2\pi\left(11.0\right)\left(4.25\right)\left(0.108\right)^2 \dot{Q}_c \int_0^\infty \exp\left(-0.6931 \ \eta^2\right) \cdot \exp\left(-0.6931 \ \left(\eta/\alpha\right)^2\right) \cdot \frac{T_\infty}{T}\left(\frac{T_0}{T_\infty}\right)^{2n} \eta \, d\eta \quad , \tag{2-19}$$

where

$$\eta = r / b_U \tag{2-20}$$

and Eqs. 2-14, 2-2, 2-15, and 2-7 have been used respectively to express ΔT, ΔT_0, u, and u_0. The plume half width, $b = b_U$, has been introduced by replacing Eq. 2-12 with the following form, in which the value of the exponent of the temperature ratio is left unassigned:

$$b_U = 0.108 \cdot \left(\frac{T_0}{T_\infty}\right)^n \left(z - z_0\right) \quad . \tag{2-21}$$

The expression for the enthalpy flux in the plume, given as Eq. 2-19, can be rewritten in more compact form as:

$$\dot{Q}_{ent} / \dot{Q}_c = 2\pi\left(11.0\right)\left(4.25\right)\left(0.108\right)^2 \left\{I\right\} \ , \tag{2-22}$$

where the integral, {*I*}, is:

$$\{I\} = \int_0^\infty \exp\left(-0.6931\ \eta^2\right) \cdot \exp\left(-0.6931\ (\eta/\alpha)^2\right) \cdot \frac{\left(1+\Delta T_0/T_\infty\right)^{2n}}{1+\left(\Delta T_0/T_\infty\right)\left(\Delta T/\Delta T_0\right)} \eta\, d\eta \quad . \qquad 2\text{-}23$$

In Eq. 2-22, the ratio between the flux of enthalpy in the plume and the convective HRR is written by separating out the part that depends on the constants in the correlation formulas (11.0, 4.25 and 0.108) from the integral, which contains the details of the radial variation of the velocity and temperature profiles. Since the enthalpy flux should remain invariant over the non-reacting portion of the plume, the integral {*I*} should be constant over the range of $\Delta T_0/T_\infty$ corresponding to those conditions. This hypothesis will be tested by the results shown in the next figure, which presents the calculated enthalpy flux divided by its value for negligible temperature rise in the plume. The estimates are based on the value of 0.92 for α, as recommended in Ref. [6].

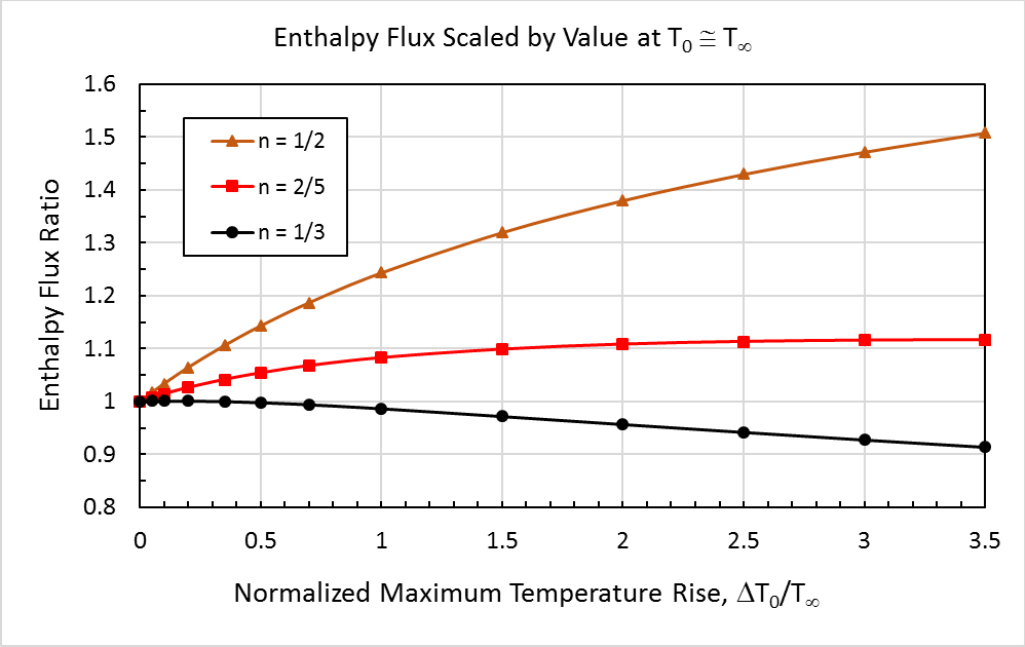

Figure 2-1: Enthalpy flux scaled by the value for negligible temperature rise in the plume, shown for different levels of temperature rise on the plume axis (α = 0.92).

The top curve in Fig. 2-1 corresponds to the case where the plume width is estimated based on Eq. 2-12 (i.e., *n* = 1/2). As can be seen, the integral ratio increases from the colder regions of the plume ($\Delta T_0/T_\infty \cong 0$) to the location of the continuous flame ($\Delta T_0/T_\infty$ = 3.5). Even at the end of the intermittent flame region, corresponding to $\left(z-z_0\right)/\dot{Q}_c^{2/5} \cong 0.2\ m/kW^{2/5}$, at which point it is $\Delta T_0/T_\infty \cong 1.5$, the value of the integral is 32% higher than at the limit of negligible temperature rise. This result is physically incorrect. In other words, the accepted fire plume correlations are not consistent with the notion of a constant enthalpy flux in the non-reacting portion of the flow. The relevant issue is to identify which part of the correlation is mainly responsible for the observed discrepancy.

As already noted, the constants in Eqs. 2-2, 2-7 and 2-12 (i.e., 11.0, 4.25 and 0.108), while affecting the value of the $\dot{Q}_{ent}/\dot{Q}_c$ ratio, do not appear in the {*I*} integral and therefore are not potential candidates for resolving the discrepancy. The {*I*} integral depends on the shape of the radial profiles (assumed Gaussian), on the factor α and on the exponent *n*. Challenging the profile assumption is difficult since the choice of the Gaussian is supported by measurements [6] and it is doubtful that its replacement would provide a better fit to the data. The effect of changing the value of α within a reasonable range has been found to be negligible. That leaves the exponent *n* as the best candidate for consideration.

The other two curves in Fig. 2-1 show that better physical consistency is achieved if lower values are assumed for the constant, *n*, in the expression for the plume half width. Slightly decreasing values of the integral ratio for increasing $\Delta T_0/T_\infty$ are obtained with *n* = 1/3. The fact that the integral ratio is very close to 1 in the non-reacting portion of the plume ($0 < \Delta T_0/T_\infty < 1.5$), confirms that the choice of *n* = 1/3 is preferable to the literature recommendation of *n* = 1/2.

Having taken care of ensuring approximate conservation of the enthalpy flux over the height of the non-reacting portion of the plume, the next step is to determine whether the absolute magnitude of the enthalpy flux is consistent with the known value of convective heat release rate. With *n* now set equal to 1/3, the expression for the integral becomes:

$$\{I\} = \int_0^\infty \exp\left(-0.6931\ \eta^2\right) \cdot \exp\left(-0.6931\ (\eta/\alpha)^2\right) \cdot \frac{\left(1+\Delta T_0/T_\infty\right)^{2/3}}{1+\left(\Delta T_0/T_\infty\right)\exp\left(-0.6931\ (\eta/\alpha)^2\right)} \eta\, d\eta \qquad 2\text{-}24$$

At the limit of negligible temperature rise ($\Delta T_0/T_\infty \cong 0$), the above integral can be solved analytically, and its value is {*I*} = 0.3307. When substituted in Eq. 2-22, the result is:

$$\dot{Q}_{ent} = 1.133\, \dot{Q}_c \qquad . \qquad 2\text{-}25$$

The above equation states that the convective heat flux implied by the correlations for vertical velocity and temperature rise in the fire plume is 13.3% higher than the nominal convective heat release rate of the fire. This inconsistency is further aggravated by the fact that turbulent fluctuations, which contribute about 6% to the value calculated on the basis of average quantities (cf., Section B.1 in Appendix B), should be added to the right-hand side of the above equation. In order to provide consistency, Eq. 2-25 should read:

$$\dot{Q}_{ent} \cong 0.94\, \dot{Q}_c \qquad . \qquad 2\text{-}26$$

The thermal plume measurements reported in Ref. [6] suggest the values of 9.1 and 3.4 for the two constants given in Eqs. 2-2 and 2-7 as 11.0 and 4.25, respectively. The lower set of constants, if substituted in the expression for the convective heat flux, would yield:

$$\dot{Q}_{ent} = 0.750\, \dot{Q}_c \qquad , \qquad 2\text{-}27$$

a value that is significantly lower than the desired target of about 0.94. In a later reanalysis of their data [7], the same group of Ref. [6] recommended that the two constants in Eqs. 2-2 and 2-7 be set equal to

9.5 and 3.6 (the same authors found that the velocity profile is wider than the temperature profile and suggested $\alpha \cong 0.92$, as mentioned earlier). When these constants are substituted in Eq. 2-22, the result is:

$$\dot{Q}_{ent} = 0.829\, \dot{Q}_c \quad . \tag{2-28}$$

The above value is still lower than desired. It would appear that better consistency can be achieved by choosing a set of constants somewhat intermediate between those of Kung et al. [4] and the above set from Ref. [6]. We will choose here to use 10.0 and 3.9, for which Eq. 2-22 becomes:

$$\dot{Q}_{ent} = 0.945\, \dot{Q}_c \quad . \tag{2-29}$$

2.5 Mass Flux

The mass flux in the fire plume is given by:

$$\dot{m} = 2\pi \int_0^\infty \rho u\, r\, dr \quad . \tag{2-30}$$

After substitution of the expressions for the various terms listed above, Eq. 2-30 becomes:

$$\dot{m} = 2\pi\, \rho_\infty\, u_0 \left(z - z_0\right)^2 (0.108)^2 \int_0^\infty \exp\left(-0.6931\eta^2\right) \cdot \frac{T_\infty}{T} \left(\frac{T_0}{T_\infty}\right)^{2n} \eta\, d\eta \quad . \tag{2-31}$$

Again, assuming a small temperature rise above ambient, namely $T_0/T_\infty \cong 1$, the integral in Eq. 2-31 can be solved analytically, yielding:

$$\dot{m} = 0.05287\, \rho_\infty\, u_0 \left(z - z_0\right)^2 \quad . \tag{2-32}$$

Unlike the enthalpy flux, which remains constant in the fire plume, for a given convective HRR, $\dot{Q}_c$, the mass flux increases by the 5/3 power of height (cf. Eq. 2-7 for the -1/3 power dependence of u_0 on z-z_0).

2.6 Momentum Flux

The momentum flux in the fire plume is given by:

$$\dot{W} = 2\pi \int_0^\infty \rho u^2\, r\, dr \quad . \tag{2-33}$$

Equations 2-17 and 2-33 can be seen to be quite similar, with the term $c_p\, \Delta T$ in the former being replaced by u in the latter. If the excess temperature and velocity can be assumed to have the same profiles, i.e., same shape and width, then the momentum flux can be written by reference to the centerline values for those two quantities as:

$$\dot{W} \cong \frac{u_0}{c_p \, \Delta T_0} \dot{Q}_c \quad . \tag{2-34}$$

If the expressions for ΔT_0 and u_0, from Eqs. 2-2 and 2-7 with the updated constants 10.0 and 3.9, in the case of the thermal plume, are substituted in Eq. 2-34, then a relationship is obtained for $\dot{W}$ as a function of $\dot{Q}_c$ and $(z\text{-}z_0)$:

$$\dot{W} \cong \frac{3.9}{10.0} \cdot \left(\frac{g^2 \rho_\infty}{c_p^2 T_\infty^2} \right)^{1/3} \dot{Q}_c^{2/3} \left(z - z_0 \right)^{4/3} \quad . \tag{2-35}$$

When extended to the flame region, substitution of Eqs. 2-1 and 2-10 into Eq. 2-34 leads to:

$$\dot{W} \cong \frac{3.9}{\sqrt{3.5 \cdot 10.0}} \cdot \frac{1}{c_p \, T_\infty} \sqrt{g \left(z - z_0 \right)} \dot{Q}_c \quad . \tag{2-36}$$

As was done in the case of the enthalpy flux, it is interesting to verify the extent to which the plume correlations satisfy the momentum equation. Unlike the enthalpy flux, which is conserved, the plume momentum increases with height because of the work done by gravity. The rate of change of the plume momentum in the vertical direction is equal to the integral of the buoyancy force over the plume cross-section:

$$\frac{d\dot{W}}{dz} = 2\pi \int_0^\infty \Delta\rho \, g \, r \, dr \quad . \tag{2-37}$$

When equations for temperature rise (Eqs. 2-2 and 2-14 with the constant set to 10.0) and velocity (Eqs. 2-7 and 2-15 with the constant set to 3.9) are substituted in the above expression and after simplification of terms that appear on both sides, the equality becomes:

$$\begin{aligned} &(3.9)^2 \, \frac{d}{dz} \left\{ \left(z - z_0 \right)^{-2/3} \int_0^\infty \exp\left(-2 \cdot 0.6931 \, \left(r / b_u \right)^2 \right) \cdot \frac{T_\infty}{T} \, r \, dr \right\} = \\ &(10.0) \left(z - z_0 \right)^{-5/3} \int_0^\infty \exp\left(-0.6931 \, \left(r / b_T \right)^2 \right) \cdot \frac{T_\infty}{T} \, r \, dr \end{aligned} \quad . \tag{2-38}$$

The above equality cannot be solved easily, owing to the dependence of terms like T/T_∞ on both radius, r, and height, z. However, in the simple case of small temperature differences where $T \cong T_0 \cong T_\infty$, the integrals can be solved, yielding:

$$\frac{2}{3}(3.9)^2 = (10.0) \, 0.92^2 \quad . \tag{2-39}$$

Since the left-hand side is equal to 10.1 and the right side to 8.5, the equality is not satisfied by a discrepancy of about 19%. If the previous set of constants (4.25 and 11.0) had been used, the discrepancy between the two sides of the equations would have been 30%. This result shows that the plume equations with the recommended new constants, while offering an improvement by approximately satisfying the momentum balance, are still not rigorously correct. Nevertheless, no further refinement has been deemed necessary at this point.

2.7 Summary of Fire Plume Analysis

The analysis detailed above has quantified the degree to which recommended correlations for temperature rise and vertical velocity in buoyant fire plumes satisfy basic conservation of energy and momentum. First, the vertical variation of enthalpy flux was considered, with the finding that reasonable constancy over the non-reacting portion of the flow could be achieved by changing the exponent of the temperature ratio term in Eq. 2-12 for the half width of the velocity profile from 1/2 to 1/3, namely:

$$b_U = b \ = 0.108 \cdot \left(\frac{T_0}{T_\infty} \right)^{1/3} \left(z - z_0 \right) \quad . \tag{2-40}$$

The second step involved ensuring consistency between the integrated enthalpy flux and the prescribed convective heat release rate of the source. In that part of the analysis, it was found that the two constants 11.0 and 4.25, respectively in Eqs. 2-2 and 2-7 for the maximum temperature rise and vertical velocity, should be replaced by 10.0 and 3.9, i.e.:

$$\Delta T_0 = 10.0 \cdot T_\infty \left(\frac{R^2}{g\, c_p^2\, p_\infty^2\, M^2} \right)^{1/3} \dot{Q}_c^{2/3} \left(z - z_0 \right)^{-5/3} \quad . \tag{2-41}$$

and

$$u_0 = 3.9 \cdot \left(\frac{g\, R}{c_p\, p_\infty\, M} \right)^{1/3} \dot{Q}_c^{1/3} \left(z - z_0 \right)^{-1/3} \quad . \tag{2-42}$$

The simplified form of the equations resulting from this choice is reported in Appendix A.

3. **Ceiling Layer Correlations**

The analysis presented in the previous chapter for the fire plume correlations will now be repeated for the ceiling layer, by tackling first the correlations reported in Ref. [4]. The analysis using a different set proposed by Heskestad [8] and Alpert [2] will be presented in the following section.

3.1 Kung, You and Spaulding Treatment

3.1.1 Temperature Rise

The maximum temperature rise in the ceiling layer as a function of radial distance from the fire axis is given in Ref. [4] by:

$$\Delta T_m = \Delta T_{0,H} \exp\left[-0.66 \left(\frac{r}{b_{CL}} - 1.5 \right)^{1/2} \right] \qquad \text{for } r > 1.5 \cdot b_{CL} \text{ ,} \qquad \text{3-1}$$

where r is the distance from the axis of the plume and $\Delta T_{0,H}$ is the temperature rise on the fire plume centerline at the height of the ceiling (cf. Eq. 2-2 with z set equal to H):

$$\Delta T_{0,H} = 11.0 \cdot T_\infty \left(\frac{R^2}{g\, c_p^2\, p_\infty^2\, M^2} \right)^{1/3} \dot{Q}_c^{2/3} \left(H - z_0 \right)^{-5/3} \quad . \qquad \text{3-2}$$

The temperature variation with distance down from the ceiling, y, is:

$$\Delta T = \Delta T_m \exp\left[-\left(\frac{y - 102mm}{\delta_T} \right)^2 \right] \qquad \text{for } y > 102 \text{ mm} \text{ ,} \qquad \text{3-3}$$

where δ_T is the depth of the layer and b_{CL} is a scaling length for the ceiling layer. Both will be discussed below.

3.1.2 Horizontal Velocity

The maximum horizontal velocity in the ceiling layer as a function of radial distance from the fire axis is given by:

$$u_m = u_{0,H} \exp\left[-0.44 \left(\frac{r}{b_{CL}} - 1.5 \right)^{0.57} \right] \qquad \text{for } r > 1.5 \cdot b_{CL} \text{ ,} \qquad \text{3-4}$$

where $u_{0,H}$ is the vertical velocity on the fire plume centerline at the height of the ceiling (cf. Eq. 2-7 with z set equal to H):

$$u_{0,H} = 4.25 \cdot \left(\frac{g\,R}{c_p\,p_\infty\,M} \right)^{1/3} \dot{Q}_c^{1/3} \left(H - z_0 \right)^{-1/3} \quad . \tag{3-5}$$

The velocity variation with distance down from the ceiling, *y*, is:

$$u = u_m \exp\left[-\left(\frac{y - 102mm}{\delta_U} \right)^2 \right] \qquad \text{for } y > 102 \text{ mm} \ , \tag{3-6}$$

where δ_U is the depth of the layer.

3.1.3 Ceiling Layer Radial Length Scale

The quantity b_{CL} is a scaling length for the ceiling layer. The standard approach has been to set this quantity equal to the half-width of the plume at the ceiling, *b*, for which a general expression has already been provided as Eq. 2-12. On this basis, it is:

$$b_{CL} = 0.108 \cdot \left(\frac{T_{0,H}}{T_\infty} \right)^{1/2} \left(H - z_0 \right) \qquad . \tag{3-7}$$

3.1.4 Ceiling Layer Depth

The depth of the ceiling layer is obtained from the following relationships, which are largely based on Refs. [4] and [1]. Modifications to these formulas documented in Ref. [3] to correct the anomalous behavior of these expressions at large ceiling heights will not be included in the present evaluation.

$$\delta_T = b_{\Delta T} \left[0.32 + s \left(\frac{r}{b_{CL}} - 3.1 \right) \right] \qquad \text{for } r > 3.1 \cdot b_{CL} \ , \tag{3-8}$$

$$s = -0.0097 - 0.0013 \frac{H_{cc}\,[m]}{1.32} + 0.0059 \left(\frac{H_{cc}\,[m]}{1.32} \right)^2 \quad , \tag{3-9}$$

$$\delta_U = 0.67\ \delta_T \quad , \tag{3-10}$$

where the additional variables are:

- H_{cc} ceiling clearance above fuel array [m];
- δ_T ceiling layer thermal depth [m];
- δ_U velocity depth of the ceiling layer [m].

3.1.5 Enthalpy Flux

The enthalpy flux in the ceiling layer is given by:

$$\dot{Q}_{ent} = 2\pi\, r \int_0^H c_p\, \Delta T\, \rho u\, dz \quad , \tag{3-11}$$

or

$$\dot{Q}_{ent} = 2\pi\, r\, \rho_\infty T_\infty\, c_p \int_0^H \frac{\Delta T}{T} u\, dz \quad . \tag{3-12}$$

The structure of Eq. 3-11 is very similar to that of Eq. 2-17, with the exception that the enthalpy flux is calculated through a cylindrical surface at distance *r* from the axis of the fire plume and over the height of the ceiling layer. Furthermore, temperature rise, ΔT, and horizontal velocity, *u*, are now given by Eqs. 3-1 to 3-3 and 3-4 to 3-6, respectively. Under an adiabatic ceiling, this quantity remains constant. For the more practical conditions where heat losses to the ceiling are present, the enthalpy flux is expected to be some decreasing function of radius, *r*.

The internal consistency of the correlations presented above for temperature rise and horizontal velocity will now be checked for the ceiling layer. By substituting in Eq. 3-12 the expressions for temperature rise and velocity, one obtains:

$$\begin{aligned}\dot{Q}_{ent} = {} & 2\pi\, r\, (11.0)(4.25)\, \dot{Q}_c^{\,2}\, (H - z_0)^{-2} \\ & \exp\left[-0.44 \left(\frac{r}{b_{CL}} - 1.5 \right)^{0.57} \right] \cdot \exp\left[-0.66 \left(\frac{r}{b_{CL}} - 1.5 \right)^{0.5} \right] \quad , \\ & \int_0^H \exp\left[-\left(\frac{y - 102\ mm}{\delta_T} \right)^2 \right] \cdot \exp\left[-\left(\frac{y - 102\ mm}{\delta_U} \right)^2 \right] \cdot \frac{T_\infty}{T}\, dz\end{aligned} \tag{3-13}$$

where the distance *y* is:

$$y = H - z \quad . \tag{3-14}$$

Equation 3-13 can be rewritten by introducing the expression for b_{CL} from Eq. 3-7 and, after some rearranging of terms, one obtains:

$$\begin{aligned}\dot{Q}_{ent} / \dot{Q}_c = {} & 2\pi \frac{r}{b_{CL}} (11.0)(4.25)(0.108) \left(\frac{T_{0,H}}{T_\infty} \right)^{1/2} \\ & \exp\left[-0.44 \left(\frac{r}{b_{CL}} - 1.5 \right)^{0.57} \right] \cdot \exp\left[-0.66 \left(\frac{r}{b_{CL}} - 1.5 \right)^{0.5} \right] \quad . \\ & \int_0^H \exp\left[-\left(\frac{H - z - 102\, mm}{\delta_T} \right)^2 \right] \cdot \exp\left[-\left(\frac{H - z - 102\, mm}{\delta_U} \right)^2 \right] \cdot \frac{T_\infty}{T} \frac{dz}{H - z_0}\end{aligned} \tag{3-15}$$

a.

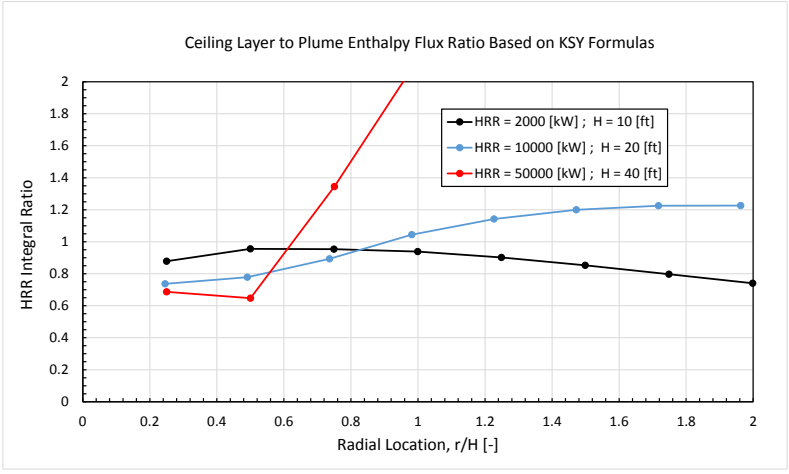

b.

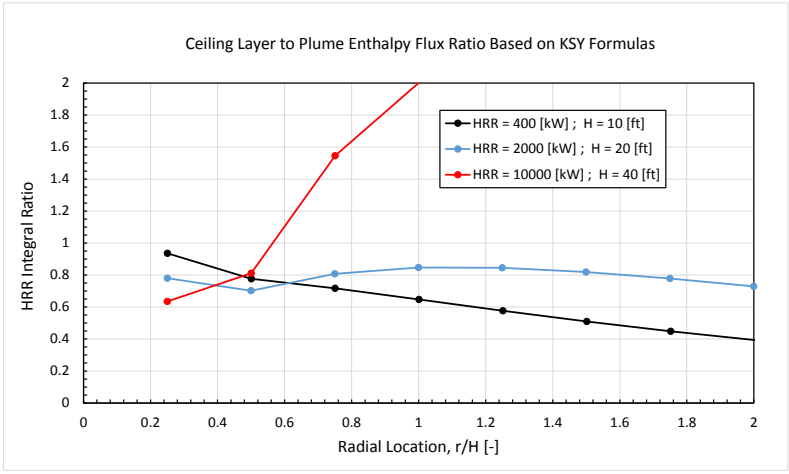

c.

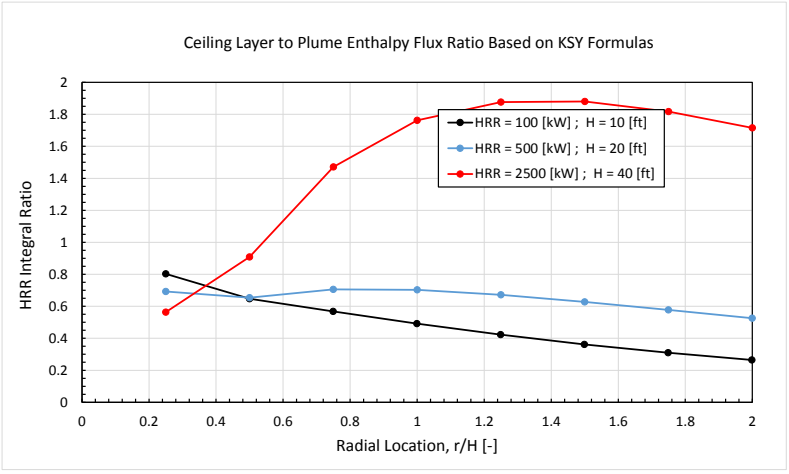

Figure 3-1: Ratio of Enthalpy Flux in the Ceiling Layer to the Convective Heat Release Rate of the Source Fire (Kung et al. formulas). Peak Temperature Rise at the Ceiling Center, $\Delta T_{0,H}$: a. ~625°C (1,125°F); b. ~215°C (390°F); c. ~85°C (150°F).

The left-hand side of the equation is the ratio between the enthalpy flux in the ceiling layer and the convective heat release rate of the fire. If the ceiling is adiabatic, this ratio is supposed to be equal to 1.

If there are heat losses, then the ratio should take some value less than 1. It should also be noted that distances generally appear as scaled quantities. In the case of the layer depths, δ_T and δ_U, the formula by Kung et al. (Eqs. 3-8 and 3-9) imply a dependence on (H - z_0) through b_{CL} (Eq. 3-7), but not direct scaling as in the case of other correlations to be discussed later. Even though an analytical solution could be obtained for the limiting case of small temperature rises, Eq. 3-15 will be solved numerically and the results presented in the plots in Fig. 3-1.

There are three plots in the figure. They show the value of the ratio $\dot{Q}_{ent}/\dot{Q}_c$ (cf. Eq. 3-15) between the enthalpy flux in the ceiling layer and the convective HRR of the fire at different radial locations. Each plot has three curves for ceiling heights of 10, 20 and 40 ft (3.0, 6.1 and 12.2 m), but with the HRR of the fire adjusted to provide approximately the same temperature rise at the point of plume impingement on the ceiling. The strongest fires are shown in the top plot ($\Delta T_{0,H} \cong$ 625°C (1,125°F), $\Delta T_{0,H} / T_\infty \cong 2.1$), the weakest at the bottom ($\Delta T_{0,H} \cong$ 85°C (170°F), $\Delta T_{0,H} / T_\infty \cong 0.28$). The calculations were done for a pool fire with its diameter adjusted such that the virtual source was located at the surface of the pool (z_0 = 0, Eqs. 2-3 and 2-4).

The expectation is that the enthalpy ratio, $\dot{Q}_{ent}/\dot{Q}_c$, would be equal to about 1 and remain approximately constant over the range of radii covered in the abscissa (H is the height of the ceiling above the pool surface). The plots do not bear out that expectation: as can be seen, there are wide variations in the enthalpy ratio, particularly in the case of H = 40 ft (12.2 m), where values of 2 and greater are obtained. This problem is largely attributable to the fact that the formulas in Eqs. 3-8 and 3-9 yield unreasonably large values for δ_T and δ_U when used beyond the range of the underlying data (H = 5-20 ft (1.5-6.1 m)). This issue had already been identified and an empirical fix had been proposed in Ref. [3]. However, it does appear that, even within its range of applicability, the formulation by Kung et al. [4] is not entirely reliable. For example, note the very low values of the enthalpy ratio for intermediate (b) and low (c) temperature rise.

Given this result, further analysis of these correlations has not been pursued.

3.2 Heskestad and Alpert Treatment

Different correlations from those used in the previous section have been introduced by Alpert and Heskestad and are documented in Refs. [2], [8] and [9]. They will be used in the remainder of this section to perform an analysis of the enthalpy flux in the ceiling layer.

3.2.1 Temperature Rise

The correlation recommended for the maximum temperature rise in the ceiling layer, as reported in the paper by Heskestad [8], reads:

$$\Delta T_m^* = \left(0.225 + 0.27 \frac{r}{H} \right)^{-4/3} \quad \text{for } 0.2 \leq r/H < 4.0 \text{ ,}$$
$$\Delta T_m^* = 6.3 \quad \text{for } r/H < 0.2 \text{ ,} \qquad \text{3-16}$$

where the first expression describes how the maximum temperature rise in the ceiling layer decays with distance from the fire axis, whereas the second applies to the turning region close to the axis. The latter can be taken to be equal to the maximum temperature rise in the fire plume at the ceiling height. The dimensionless maximum temperature rise, ΔT_m^*, is given by:

$$\Delta T_m^* = \frac{\Delta T_m / T_\infty}{\left(\dot{Q}^*\right)^{2/3}} \quad , \tag{3-17}$$

and $\dot{Q}^*$ by:

$$\dot{Q}^* = \frac{\dot{Q}}{\sqrt{g}\, c_p\, \rho_\infty\, T_\infty\, H^{5/2}} \quad . \tag{3-18}$$

It should be noted that there is a small anomaly at the merging of the two expressions given as Eq. 3-16. At the point of its lower limit of validity, *r/H* = 0.2, the first expression takes the value 5.49 (instead of 6.3). The value of 6.3 would be reached by the correlation for *r/H* = 0.098.

If Eqs. 3-17 and 3-18 are substituted into the second formula in Eq. 3-16, and after rearranging terms, one obtains the following expression:

$$\Delta T_{0,H} = 6.3 \cdot T_\infty \left(\frac{R^2}{g\, c_p^2\, p_\infty^2\, M^2} \right)^{1/3} \dot{Q}^{2/3}\, H^{-5/3} \qquad \text{for } r/H < 0.2 \quad , \tag{3-19}$$

where the subscript "*0,H*" has been used instead of "*m*" in recognition of the fact that the maximum temperature rise given in the above equation is equal to the temperature rise in the fire plume at the ceiling level.

In comparison with Eq. 3-1, Eq. 3-19 presents some differences. First, the total HRR, $\dot{Q}$, takes the place of the convective HRR, $\dot{Q}_c$. Second, the effect of the virtual source, represented by its elevation, z_0, is neglected. Third, the dimensionless constant is 6.3 instead of 11.0. If it is assumed that the convective HRR is 70% of the total,

$$\dot{Q}_c = 0.7\, \dot{Q} \quad , \tag{3-20}$$

substitution of $\dot{Q}_c$ for $\dot{Q}$ into Eq. 3-19, so that $\Delta T_{0,H}$ is now written in terms of convective HRR, makes the constant assume the value 8.0. This would be more in line with the 11.0 constant in Eq. 2-2 and with the value of 10.0 recommended at the end of the enthalpy flux analysis carried out earlier in this report for the fire plume.

Finally, in terms of $\Delta T_{0,H}$, the decay of the maximum temperature rise in the ceiling layer can be written as:

$$\Delta T_m = \Delta T_{0,H}\ \frac{1}{6.3}\left(0.225 + 0.27\,\frac{r}{H}\right)^{-4/3} \qquad \text{for } 0.2 \le r/H < 4.0\ . \qquad 3\text{-}21$$

3.2.2 Horizontal Velocity

The correlation recommended for the maximum horizontal velocity in the ceiling layer is taken from a paper by Alpert [9]. It reads:

$$\begin{aligned} u_m^* &= 1.06\left(\frac{r}{H}\right)^{-0.69} && \text{for } 0.17 \le r/H < 4.0\ , \\ u_m^* &= 3.61 && \text{for } r/H < 0.17\ , \end{aligned} \qquad 3\text{-}22$$

where the first expression describes how the maximum horizontal velocity in the ceiling layer decays with distance from the fire axis, whereas the second applies to the turning region close to the axis. The latter can be taken to be equal to the maximum vertical velocity in the fire plume at the ceiling height. The dimensionless maximum velocity, u_m^*, is given by:

$$u_m^* = \frac{u_m \big/ \sqrt{g\,H}}{\left(\dot{Q}^*\right)^{1/3}} \qquad . \qquad 3\text{-}23$$

The anomaly at the merging of the two expressions given as Eq. 3-16 for the temperature rise is not present in the two expressions describing the maximum velocity in Eq. 3-22. At the crossover point (*r/H* = 0.17), the first expression takes the value 3.60, which is essentially the same as what is given for the second expression.

If Eqs. 3-23 and 3-18 are substituted into the second formula in Eq. 3-22 and terms are rearranged, one obtains the following expression:

$$u_{0,H} = 3.61 \cdot \left(\frac{g\,R}{c_p\ p_\infty\ M}\right)^{1/3} \dot{Q}^{1/3}\ H^{-1/3} \qquad , \qquad 3\text{-}24$$

where, similar to the case of the temperature formula, the subscript "*0,H*" has been used instead of "*m*".

When compared with Eq. 3-5, Eq. 3-24 presents the same differences already noted for Eq. 3-19: the total HRR, $\dot{Q}$, takes the place of the convective HRR, $\dot{Q}_c$; the effect of the virtual source, represented by its elevation, z_0, is neglected; and the dimensionless constant is 3.61 instead of 4.25. If it is again assumed that the convective HRR is 70% of the total (cf. Eq. 3-20), after substitution of $\dot{Q}_c$ for $\dot{Q}$ into Eq. 3-24, so that u_m is now written in terms of convective HRR, the constant in the equation assumes the value 4.1. This value would be quite consistent with the 4.25 constant in Eq. 2-7 and with the value of 3.9 recommended at the end of the plume enthalpy flux analysis carried out earlier in this document.

Finally, in terms of $u_{0,H}$, the decay of the maximum horizontal velocity in the ceiling layer can be written as:

$$u_m = u_{0,H}\,\frac{1.06}{3.61}\left(\frac{r}{H}\right)^{-0.69} \qquad \text{for } 0.17 \le r/H < 4.0\ . \qquad 3\text{-}25$$

3.2.3 Ceiling Layer Radial Length Scale

Equations 3-21 and 3-25 have already introduced the ceiling clearance above the fuel, *H*, as the length scale for the excess temperature and velocity decay in the ceiling layer. For the case of strong plumes (flames touching the ceiling and/or extending under the ceiling), Heskestad and Hamada [10] have proposed the following correlation for the temperature:

$$\Delta T_m = \Delta T_{0,H}\left\{1.92\left(\frac{r}{b}\right)^{-1} - \exp\left[1.61\left(1-\frac{r}{b}\right)\right]\right\} \qquad \text{for } 1 \le r/b < 40\ . \qquad 3\text{-}26$$

The radius, *b*, where the velocity of the impinging plume is equal to one half of the centerline value, is given in Ref [10] by:

$$b = 0.42\cdot\left[\left(c_p\,\rho_\infty\right)^{4/5}\,T_\infty^{3/5}\,g^{2/5}\right]^{-1/2}\,\frac{T_{0,H}^{1/2}\,\dot{Q}_c^{2/5}}{\Delta T_{0,H}^{3/5}}\ . \qquad 3\text{-}27$$

After some manipulation, which involves introducing the expression for $\Delta T_{0,H}$ from Eq. 3-19, the above expression simplifies to:

$$b = 0.42\cdot 6.3^{-3/5}\cdot\left(\frac{T_{0,H}}{T_\infty}\right)^{1/2} H\ . \qquad 3\text{-}28$$

When compared to Eq. 3-7 for b_{CL}, the above expression is seen to have the same structure, except for the neglect of the virtual source effect and for the difference in the multiplying constant ($0.42\cdot 6.3^{-3/5}$ = 0.139 instead of 0.108). If 6.3 is replaced with 8.0, as suggested earlier, the constant in Eq. 3-28 becomes 0.121, which is in better agreement with the value of 0.108 of Eq. 3-7.

3.2.4 Ceiling Layer Depth

The thickness of the ceiling layer, defined by Alpert [9] as the distance below the ceiling where the excess gas temperature drops to 1/*e* of its maximum value, is given by:

$$\delta_T / H = 0.112\cdot\left[1-\exp\left(-2.24\,r/H\right)\right] \qquad \text{for } 0.26 \le r/H \le 2.0\ . \qquad 3\text{-}29$$

The same reference appears to suggest that the thickness of the velocity layer is:

$$\delta_U = 0.8\,\delta_T\ . \qquad 3\text{-}30$$

a.

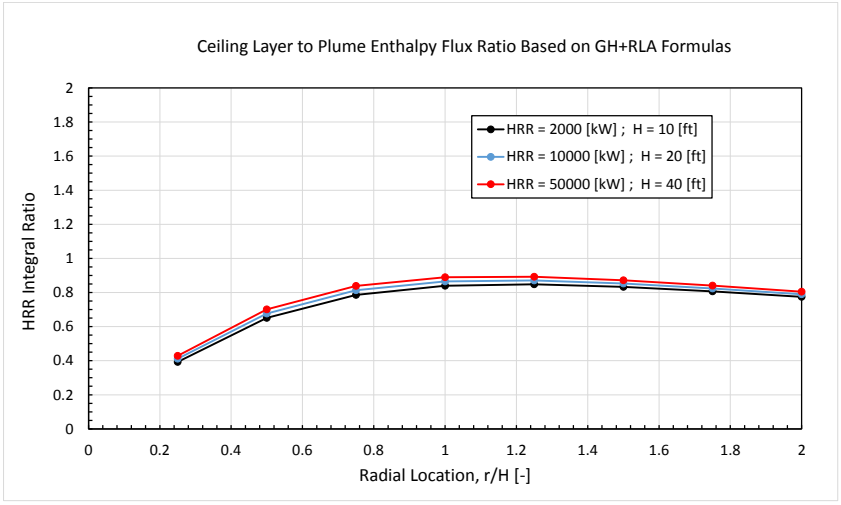

b.

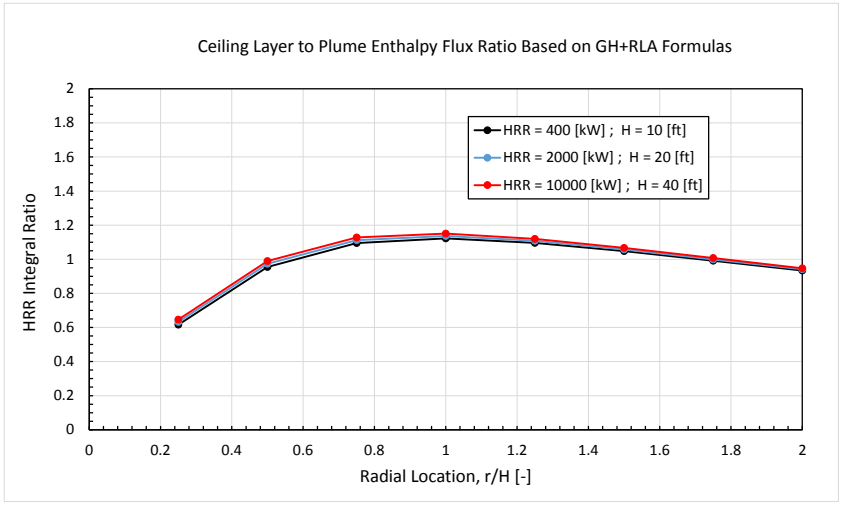

c.

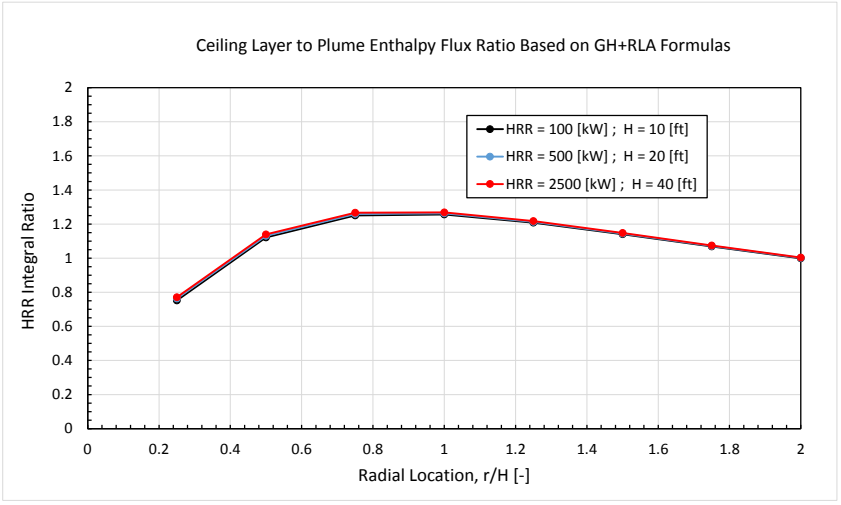

Figure 3-2: Ratio of Enthalpy Flux in the Ceiling Layer to the Convective Heat Release Rate of the Source Fire (Heskestad/Alpert formulas). Peak Temperature Rise at the Ceiling Center, $\Delta T_{0,H}$: a. ~500°C (900°F); b. ~170°C (306°F); c. ~68°C (122°F).

3.2.5 Enthalpy Flux

The estimate of the enthalpy flux in the ceiling layer is still based on Eq. 3-12, but now with Eqs. 3-21, 3-25, 3-29 and 3-30 providing the expressions for peak temperature rise, horizontal velocity, and thickness of the thermal and velocity layer. The values calculated for the enthalpy ratio, $\dot{Q}_{ent}/\dot{Q}_c$, are shown in Fig. 3-2 for the same fire sizes used for the curves in Fig. 3-1. In this case, the predictions are better behaved. For example, for the same maximum temperature value at the center of the layer (data in the same plot), there is essentially no difference among the curves. This can be taken as indication of appropriate scaling. However, there are still some issues. The first is that the enthalpy ratio is seen to increase up to about $r/H \cong 1$, something that is physically hard to explain. The second issue is that the ratio reaches above 1, a fact that is physically incorrect, to values that are higher for lower temperature rises in the ceiling layer. Finally, the enthalpy ratio is seen to decrease for $r/H > 1$: this would be consistent with the presence of non-adiabatic effects, though Alpert [9] indicates that such effects should be negligible up to $r/H = 3$.

Possible approaches to correct these anomalies will be discussed next.

3.3 Proposed Modified Treatment

The first step in this analysis has considered correlations for excess temperature and vertical velocity in the fire plume. The previous two sections have detailed the performance of two sets of correlations for the profiles of horizontal velocity and temperature rise in ceiling layers. The evaluations have been carried out by considering the behavior of the correlations in terms of conservation of enthalpy flux and momentum in the fire plume, and enthalpy flux in the ceiling layer. The result has been that, in the case of the plume, relatively small changes to two coefficients and to the exponent in the formula for the variation of plume width with height have been sufficient to ensure satisfactory compliance with energy and momentum conservation. The ceiling layer case has been found more difficult to treat.

Two treatments of the ceiling layer have been considered. The first, referred to by the KYS acronym, is based on the work of Ref. [4]. The variation of the enthalpy flux along the radius has been reported in Fig. 3-1. Significant trends have been noted, with physically implausible values for the case of large ceiling clearance (40 ft [12.2 m]). The disappointing performance of the KYS correlations revealed by this analysis has been largely attributed to the formula used to calculate the depth of the layer.

A second analysis was carried out by considering a combination of plume/ceiling layer correlations by Heskestad [8] and a formula for the ceiling layer depth by Alpert [9]. The results, which have been documented in Fig. 3-2, have been more favorable than in the KYS case. However, a common feature of the calculated enthalpy flux in the ceiling layer is a significant underestimate of its value near the fire plume axis, with the deficiency extending beyond the turning region of the flow. Another issue involves values of the enthalpy flux that are greater than the convective HRR of the source fire. A third anomaly is a dependence of the peak enthalpy ratio on the maximum temperature in the layer, ranging from about 85 to 125% of convective HRR for high and low values of the maximum temperature. These observations motivate the selection of an improved treatment of the ceiling layer that overcomes the noted deficiencies. It will start with the selection of decay laws for excess temperature and velocity in the ceiling layer guided by available data.

3.3.1 Temperature/Velocity Decay in the Ceiling Layer

The decay functions proposed by Kung et al. [4] and by Heskestad [8] are shown in Fig. 3-3. These correlations have been given as Eqs. 3-1, 3-4, 3-7 and 3-16, 3-22, respectively. It should be noted that, in the case of Ref. [4], the length scale depends on the maximum temperature and the corresponding curves in the figure represent the case of $\Delta T_{0,H}/T_\infty = 0.4625$. As can be seen, there is reasonable agreement for the velocity, but the correlations for excess temperature are very different.

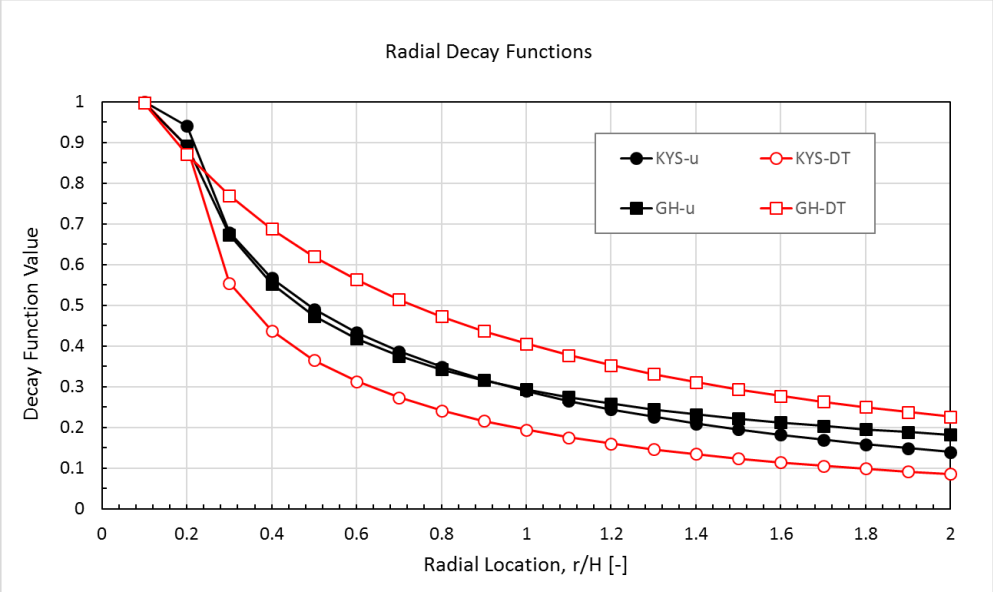

Figure 3-3: Excess Temperature and Velocity Correlations for Decay in the Ceiling Layer Used in Refs. [4] (KYS) and [8] (GH). Curves for Ref. [4] (KYS) Correspond to the Case of $\Delta T_{0,H}/T_\infty = 0.4625$.

The question of temperature decay in the ceiling layer is addressed by considering measurements for a 44-in. (1.12-m) diameter heptane pool, placed at a distance of 23.4 ft (7.13 m) from the ceiling [11]. Data from 125 thermocouples 6 in. (0.15 m) down from the ceiling[ii] were first corrected to account for heating of the ceiling using a procedure described in an internal document [12]. The correction was done by reducing the measured temperatures by ΔT_{corr}, calculated as:

$$\Delta T_{corr} = \Delta T_{clng} \sqrt{r[\,ft\,]/100} \quad , \qquad 3\text{-}31$$

where ΔT_{clng} is the temperature rise measured right above the test ceiling at its center. The corrected data were then fitted using the following exponential expression:

$$\Delta T_m = \Delta T_c \qquad \text{for } r \le b \qquad 3\text{-}32$$

[ii] These temperatures were considered sufficiently close to the ceiling to represent maximum values, a fact that was confirmed after correcting them using estimated values for the thickness of the layer.

$$\Delta T_m = \Delta T_c \exp\left[-a\left(\frac{r}{b}-1\right)^n\right] \qquad \text{for } r > b \ ,$$

with the four constants ΔT_c, a, b and n used as fitting parameters. Examples of two fitted profiles, at 100 and 600 sec into the test, are presented in Fig. 3-4, while a summary of the evolution in time of the fit parameters is given in Fig. 3-5.

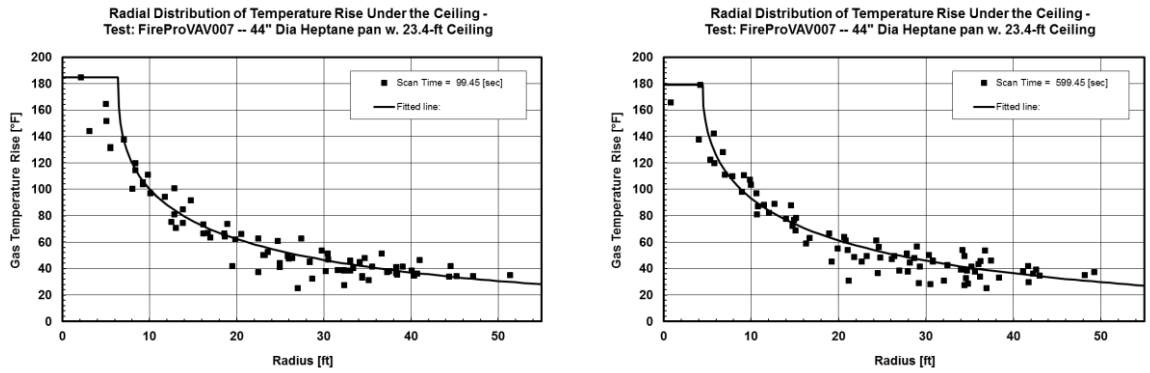

Figure 3-4: Examples of Temperature Decay Profiles in the Ceiling Layer for a 44-in. Diameter Heptane Pool under a 23.4-ft Ceiling at 100 and 600 sec in the Test.

Over the 100-600 sec time interval, the temperature curves are well approximated by:

$$\Delta T_m\ [^\circ F] = 188 \qquad \text{for } r \le 4.48 \text{ ft}$$

$$\Delta T_m\ [^\circ F] = 188 \exp\left[-0.545\left(\frac{r\ [ft]}{4.48}-1\right)^{0.506}\right] \qquad \text{for } r > 4.48 \text{ ft} \ . \qquad \text{3-33}$$

Assuming a convective heat release rate, $\dot{Q}_c$, of 1250 kW as suggested in Ref. [11], the correlation formulas from Ref. [4] (cf. Eqs. 3-1, 3-2 and 3-7) would imply:

$$\Delta T_m\ [^\circ F] = 269 \qquad \text{for } r \le 4.26 \text{ ft}$$

$$\Delta T_m\ [^\circ F] = 269 \exp\left[-0.81\left(\frac{r\ [ft]}{4.26}-1\right)^{0.5}\right] \qquad \text{for } r > 4.26 \text{ ft} \ . \qquad \text{3-34}$$

There is good agreement in the value of the power, n, inside the exponential and in the inner radius of the ceiling layer, b. There is less agreement with the other two coefficients. A detailed analysis is not possible for the velocity, because measurements in that case are available only at three radii. Nevertheless, the limited data are consistent with the following correlation:

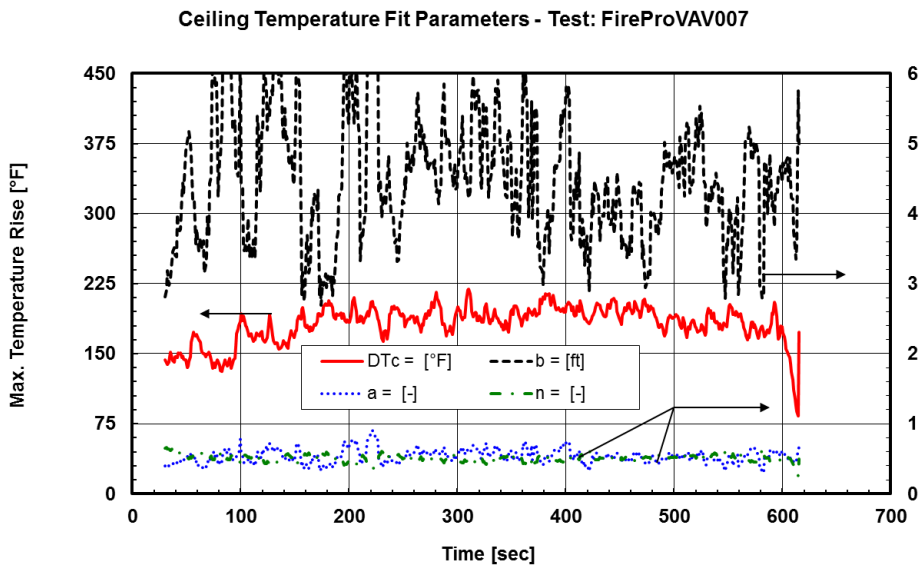

Figure 3-5: Calculated Best Fit Parameters for Assumed Exponential Decay of Excess Temperature in the Ceiling Layer for a 44-in. Diameter Heptane Pool under a 23.4-ft Ceiling.

$$u_m\,[m/s] = 5.6 \qquad \text{for } r \le 4.48 \text{ ft}$$

$$u_m\,[m/s] = 5.6\,\exp\left[-0.43\left(\frac{r\,[ft]}{4.48}-1\right)^{0.57}\right] \qquad \text{for } r > 4.48 \text{ ft} \quad . \qquad (3\text{-}35)$$

as opposed to the variation recommended in Ref. [4], which is:

$$u_m\,[m/s] = 7.4 \qquad \text{for } r \le 4.26 \text{ ft}$$

$$u_m\,[m/s] = 7.4\,\exp\left[-0.54\left(\frac{r\,[ft]}{4.26}-1\right)^{0.57}\right] \qquad \text{for } r > 4.26 \text{ ft} \quad . \qquad (3\text{-}36)$$

The same data fitting exercise was repeated assuming a power law dependence of the ceiling temperature variation with radius:

$$\Delta T_m = \Delta T_c \qquad \text{for } r \le b$$

$$\Delta T_m = \Delta T_c \left(\frac{r}{b}\right)^n \qquad \text{for } r > b \quad . \qquad (3\text{-}37)$$

Note that this fit now involves only three parameter constants, ΔT_c, b and n, instead of the four of the previously considered exponential. The data between 100 and 600 sec are well described by:

$$\Delta T_m\,[°F] = 190 \qquad \text{for } r \le 4.13 \text{ ft}$$

$$\Delta T_m\,[°F] = 190\left(\frac{r\,[ft]}{4.13}\right)^{-0.662} \qquad \text{for } r > 4.13 \text{ ft} \quad . \qquad (3\text{-}38)$$

A similar exercise performed on the more limited velocity data yields:

$$u_m\,[m/s] = 6.0 \qquad \text{for } r \le 4.13 \text{ ft}$$

$$u_m\,[m/s] = 6.0\left(\frac{r\,[ft]}{4.13}\right)^{-0.652} \qquad \text{for } r > 4.13 \text{ ft} \quad . \qquad \text{3-39}$$

The variation in time of the best fit parameters is shown in Fig. 3-6.

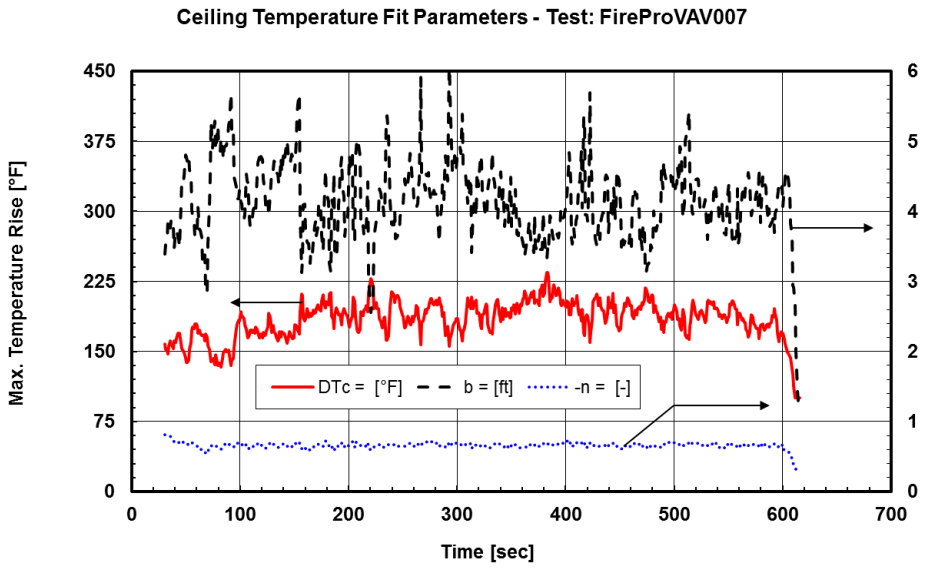

Figure 3-6: Calculated Best Fit Parameters for Assumed Power Law Decay of Excess Temperature in the Ceiling Layer for a 44-in. Diameter Heptane Pool under a 23.4-ft Ceiling.

Based on the updated fire plume correlations for ΔT_0 (Eq. 2-41) and u_0 (Eq. 2-42), the values for $\Delta T_{0,H}$ and $u_{0,H}$ are 244°F and 6.76 m/s, respectively, or about 28 and 13% higher than those recommended by the data fits. The radius of the turning region of 4.13 ft is in very good agreement with what would be calculated by setting it equal to $1.5 \cdot b_{U,H}$, which would be given as 4.0 ft by Eq. 2-40.

These results will be used in the following section to guide the choice of an appropriate set of correlations to describe the ceiling layer.

3.3.2 Overall Approach and Guiding Concepts

The approach is to select plume and ceiling layer correlations and, where necessary, modify them to develop a reliable set for use in engineering calculations. The objective will be pursued by abiding by the following guiding concepts:

1. Focus on the variation of the enthalpy flux as a meaningful performance measure;
2. Ensure consistent behavior with limited dependence of observed trends on temperature level in the layer and ceiling clearance;

3. Force energy conservation at the point of initiation of the ceiling layer (i.e., at the exit of the turning region);
4. Avoid solutions leading to physically implausible energy flux value (i.e., no values greater than convective HRR of source fire);
5. Accept a decay of enthalpy flux at increasing distances from the axis of the fire; and
6. Devise a smooth transition between the plume and the ceiling layer profiles in the turning region. (This improvement will be addressed separately in the flowing section.)

3.3.3 Detailed Strategy

The development of an improved treatment of the ceiling layer is based on the following steps:

1. The end of the plume turning region and, therefore, the beginning of the ceiling layer is at a radius r_{tr} = 1.5 $b_{U,H}$, where $b_{U,H}$ is given by Eq. 2-40 with z = H., namely:

$$r_{tr} = 0.162 \cdot \left(\frac{T_{0,H}}{T_\infty} \right)^{1/3} \left(H - z_0 \right) \quad . \tag{3-40}$$

2. The ceiling layer profile at the end of the turning region (r = r_{tr}) has peak horizontal velocity u_m = $u_{0,H}$ and peak excess temperature ΔT_m = $\Delta T_{0,H}$, where the subscript "0,H" refers to the value for the corresponding quantity on the axis at the fire plume at the ceiling level.

3. The ceiling layer profile is flat at the maximum values of velocity and temperature over a sub-layer close to the ceiling. The thickness, δ, of this sub-layer is assumed to be the same for velocity and temperature profiles and is given by the following expression:

$$\delta[m] = 0.013 \cdot \{H_0[m]\}^{-1/3} \; r[m] \quad . \tag{3-41}$$

4. The ceiling layer beneath the above layer has a half Gaussian shape, with a depth to the 1/e point of the temperature profile given by:

$$\ell_T / H_0 = 0.112 \cdot \left[1 - \exp\left(-2.24 \, r / \, H_0 \right) \right] \qquad \text{for } 0.26 \leq \; r / H_0 \leq \; 2.0 \quad . \tag{3-42}$$

and for the velocity profile:

$$\ell_U = 0.8 \cdot \ell_T \quad . \tag{3-43}$$

5. The values of ℓ_U (and ℓ_T) at the end of the turning region are selected in such a way that they make the enthalpy flux in the layer equal to the convective HRR of the fire plume.
6. The value in the turning region and the radial decay of peak excess temperature and horizontal velocity are given by:

$$\Delta T_m = \Delta T_{0,H} \quad \text{for } r/r_{tr} \le 1$$
$$\Delta T_m = \Delta T_{0,H} \left(\frac{r}{r_{tr}} \right)^{-2/3} \quad \text{for } r/r_{tr} > 1 \ , \qquad 3\text{-}44$$

and

$$u_m = u_{0,H} \quad \text{for } r/r_{tr} \le 1$$
$$u_m = u_{0,H} \left(\frac{r}{r_{tr}} \right)^{-4/5} \quad \text{for } r/r_{tr} > 1 \ , \qquad 3\text{-}45$$

where the subscript "tr" refers to the end of the turning region.

7. The vertical profiles of excess temperature and velocity in the layer are given by:

$$\Delta T = \Delta T_m \quad \text{for } 0 < y \le \delta$$
$$\Delta T = \Delta T_m \ \exp\left[-\left(\frac{y-\delta}{\ell_T} \right)^2 \right] \quad \text{for } y > \delta \ , \qquad 3\text{-}46$$

and

$$u = u_m \quad \text{for } 0 < y \le \delta$$
$$u = u_m \ \exp\left[-\left(\frac{y-\delta}{\ell_U} \right)^2 \right] \quad \text{for } y > \delta \ , \qquad 3\text{-}47$$

where y is distance down from the ceiling. In the above equations, H_0 is used to indicate the height of the ceiling above the virtual source, $(H - z_0)$.

A few words to justify the above selections are in order. First, the choice of a sub-layer of thickness, δ, growing linearly with radial distance, is a feature identified by Alpert [9]. The same paper suggests that the δ/r ratio is inversely proportional to the cube root of H_0. In this sub-layer, excess temperature and velocity should decay to the wall value and zero, respectively. For simplicity, in the following calculations, the values of these two quantities will be assumed to remain constant in the sub-layer and equal to the peak value.

Finally, the radial decay expressions for excess temperature and velocity (Eqs. 3-44 and 3-45) are also suggested by Alpert's study [9]. The exponent value of -0.8 for the velocity decay, which is lower than the value of -0.65 suggested by the data, will be justified on the basis of considerations on the radial variation of enthalpy flux. The radial decays from these power laws are shown in Fig. 3-7 where they are compared with the decay trends based on the KYS model [4]. As can be seen, there are differences, which are particularly relevant in the case of the temperature since this quantity is directly related to the estimation of convective HRR.

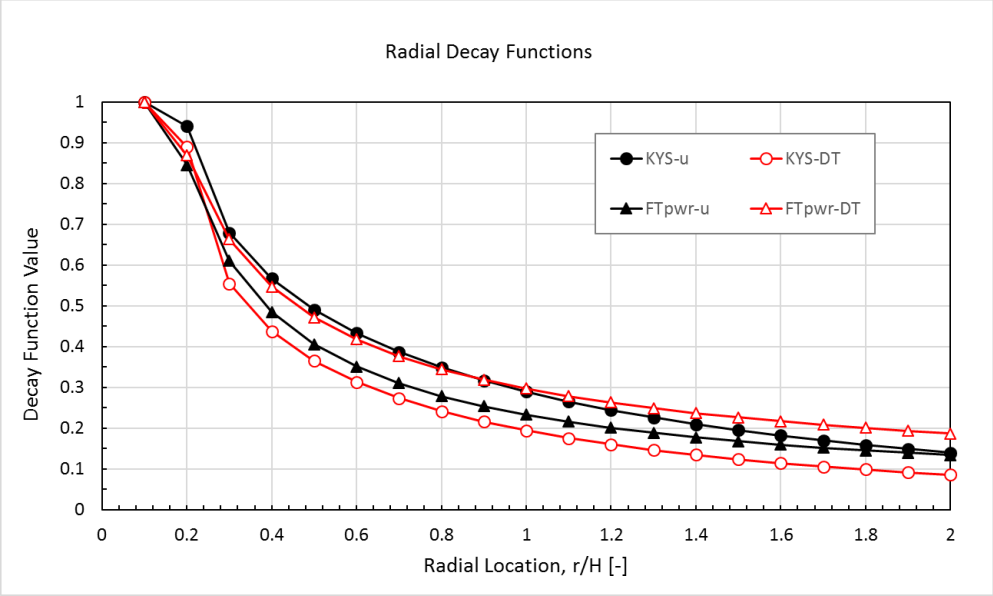

Figure 3-7: Excess Temperature and Velocity Correlations for Decay in the Ceiling Layer Used in Ref. [4] (KYS) and from the Present Work (FTpwr). Curves for Ref. [4] (KYS) Correspond to the Case of $\Delta T_{0,H}/T_\infty = 0.4625$.

3.3.4 *Small Temperature Rise Solution*

The expression for the enthalpy flux in the ceiling layer has already been introduced as Eq. 3-12, i.e.:

$$\dot{Q}_{ent} = 2\pi r \rho_\infty T_\infty c_p \int_0^H \frac{\Delta T}{T} u \, dy \quad . \tag{3-48}$$

After substituting the expressions for ΔT and u from Eqs. 3-44, 3-46, 2-41, 3-45, 3-47, and 2-42, the above equation can be written in terms of the ratio between the enthalpy flux in the ceiling layer and the convective heat release rate of the fire:

$$\dot{Q}_{ent}/\dot{Q}_c = 2\pi \frac{r}{H_0} (10.0)(3.9) \frac{\Delta T_m}{\Delta T_{0,H}} \frac{u_m}{u_{0,H}} \{I\} \, . \tag{3-49}$$

where the integral $\{I\}$ contains the only terms, which depend on distance from the ceiling, y:

$$\{I\} = \int_0^\infty \frac{T_\infty}{T} \cdot \frac{\Delta T}{\Delta T_m} \cdot \frac{u}{u_m} \cdot \frac{dy}{H_0} \quad . \tag{3-50}$$

In the above integral, there are two contributions: from the sub-layer and from the Gaussian decaying portion of the layer. They are:

$$\{I\} = \int_0^\delta \frac{T_\infty}{T_m} \cdot \frac{dy}{H_0} \quad + \quad \int_\delta^\infty \frac{T_\infty}{T} \cdot \exp\left[-\left(\frac{y-\delta}{\ell_T} \right)^2 \right] \cdot \exp\left[-\left(\frac{y-\delta}{\ell_U} \right)^2 \right] \cdot \frac{dy}{H_0} \quad . \tag{3-51}$$

In the limit of vanishing temperature differences (i.e., $T = T_m = T_\infty$), the integrals can be solved analytically, yielding:

$$\{I\} = \frac{\delta}{H_0} + \frac{1}{2}\sqrt{\frac{\pi\,\beta^2}{1+\beta^2}}\,\frac{\ell_T}{H_0} \quad . \qquad \text{3-52}$$

In the above equation, δ is given by Eq. 3-41, ℓ_T by Eq. 3-42, and $\beta = 0.8$ is the ratio of the depth of the velocity and temperature layers (cf. Eq. 3-43). Radial profiles from this analytical solution for three ceiling heights are shown in the following figure.

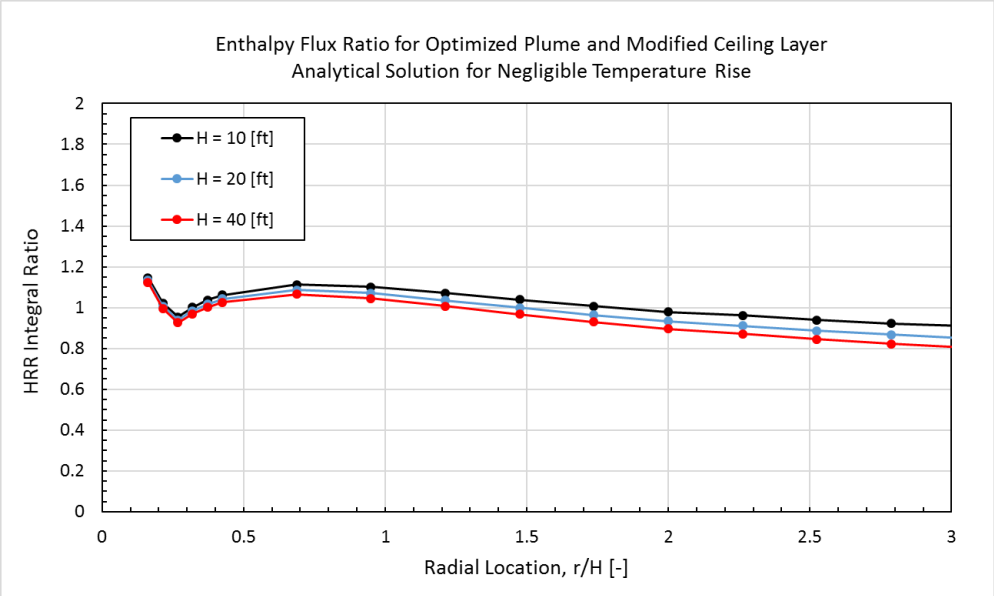

Figure 3-8: Ratio of Enthalpy Flux in the Ceiling Layer to the Convective Heat Release Rate of the Source Fire for Negligible Temperature Rise. Case of Alpert's Ceiling Depth Formula (depth ℓ_T / H_0 clipped at $r / H_0 = 0.26$ and transition region starting at $r = 1.5\ b_{U,H}$).

The calculated values have the following features:

1. The integral ratio is about 10% high at $r / H_0 = 0.75$-1.25. It is noted that this value would have been significantly higher, had an exponent of -0.65 been used in the velocity decay formula.
2. The ratio presents a minimum at the cutoff in ℓ_T / H_0 corresponding to $r / H_0 = 0.26$.

Possible fixes for the above non-desirable trends include removing the cutoff on ℓ_T / H_0, adding a term to force an increase in the depth of the layer at low radii and adjusting the distance over which the layer reaches constant thickness. To test this strategy, Eq. 3-42 is changed to:

$$\ell_T / H_0 = 0.11 \cdot \left[1 + 1.5\exp\left(-6.4\, r / H_0\right)\right] \cdot \left[1 - \exp\left(-1.8\, r / H_0\right)\right] \quad , \qquad \text{3-53}$$

and no limits are set to its range of applicability. The result from implementation of Eq. 3-53 is shown in Fig. 3-9. As can be seen, the radial variation of the enthalpy is now quite acceptable, particularly with regard to values of the ratio very close to 1 for r / H_0 up to about 1.5. The question is how applicable this result is to the more practical case of elevated ceiling layer temperatures, an issue that will be tackled next.

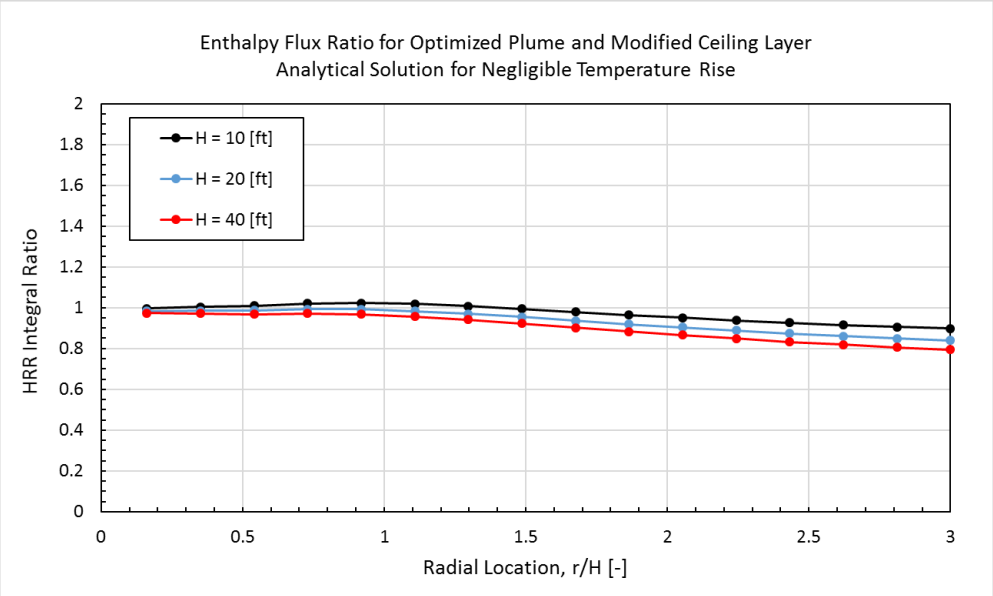

Figure 3-9: Ratio of Enthalpy Flux in the Ceiling Layer to the Convective Heat Release Rate of the Source Fire for Negligible Temperature Rise (no clipping of ℓ_T / H_0 and transition region starting at r = 1.5 $b_{U,H}$).

3.3.5 Solution for Arbitrary Temperature Rise

If the temperature rise in the ceiling layer is not negligible, Eqs. 3-49 and 3-51 are still valid, but the integral {I} now must be calculated numerically. The result is shown in Figs. 3-10 and 3-11. First, it should be noted that the curves in the plot of Fig. 3-10c approach those calculated from the analytical solution for the case of vanishingly small temperature rise in the layer, shown in Fig. 3-9. The quality of the curves, however, becomes less acceptable as the layer temperatures increase (cf. plots a. and b. in Fig. 3-10). Most notably, there is a drop in the enthalpy flux ratio at small radii, which is larger, the greater the temperature rise. This is interpreted as meaning that the layer thickness given by Eq. 3-53 is too small when temperatures are high.

a.

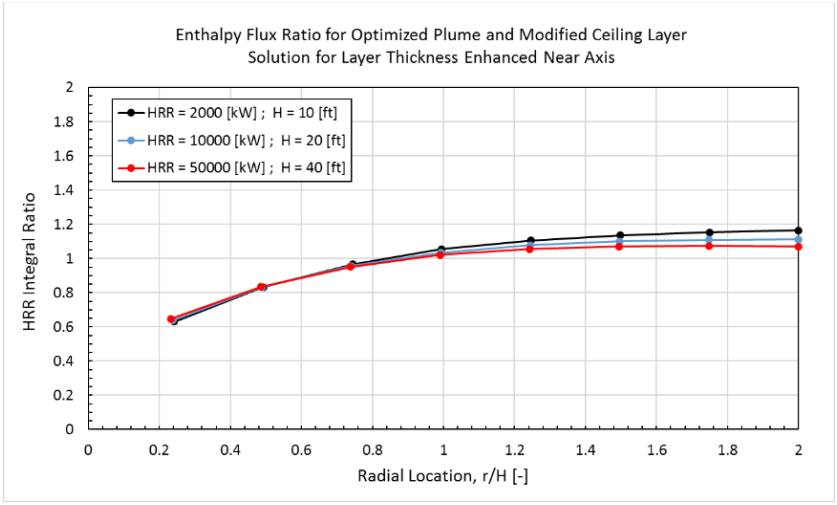

b.

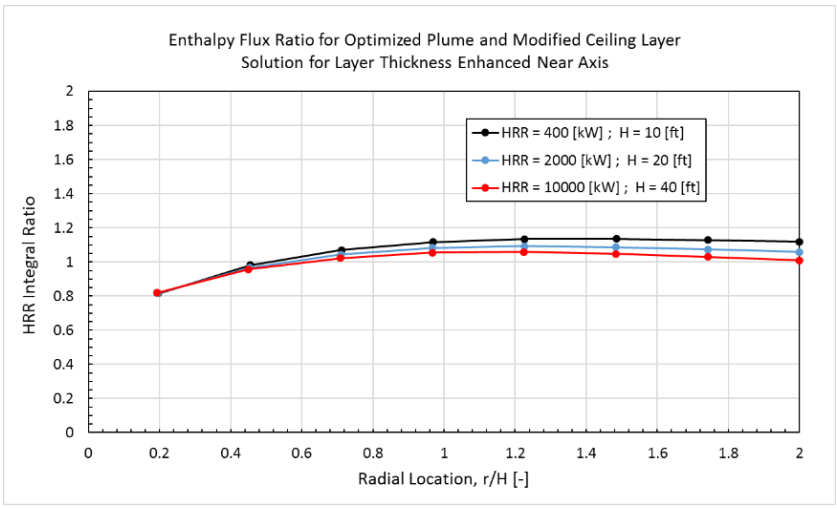

c.

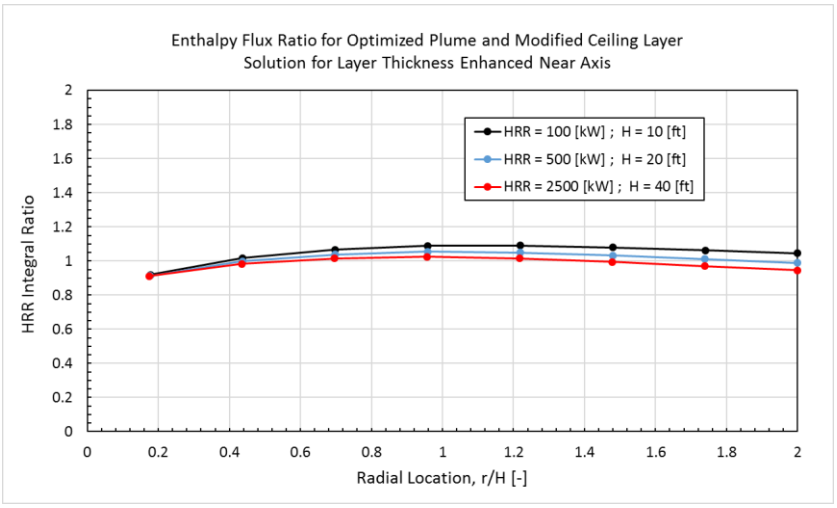

Figure 3-10: Ratio of Enthalpy Flux in the Ceiling Layer to the Convective Heat Release Rate of the Source Fire (optimized plume and modified ceiling layer). Peak Temperature Rise at the Ceiling Center, $\Delta T_{0,H}$: a. ~625°C (1,125°F); b. ~215°C (390°F); c. ~85°C (150°F).

a.

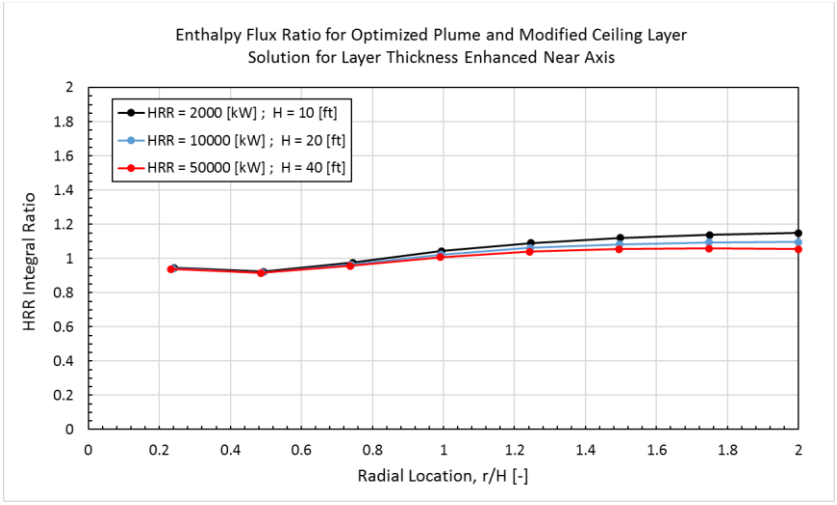

b.

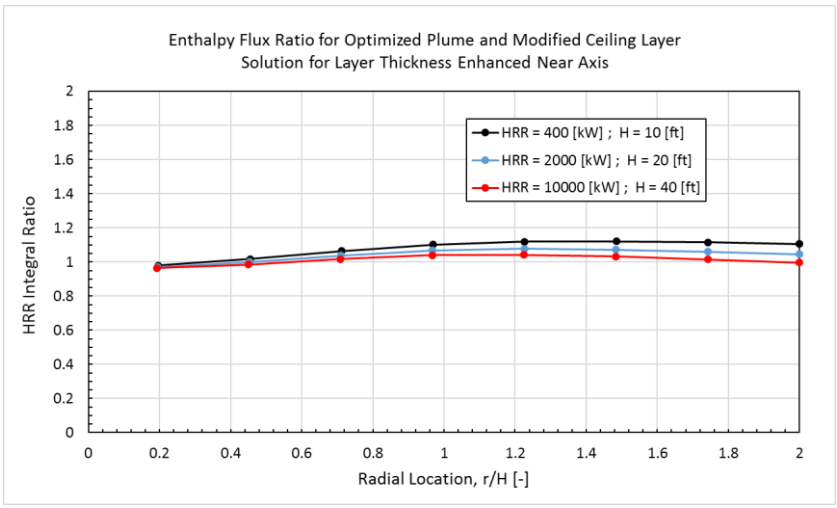

c.

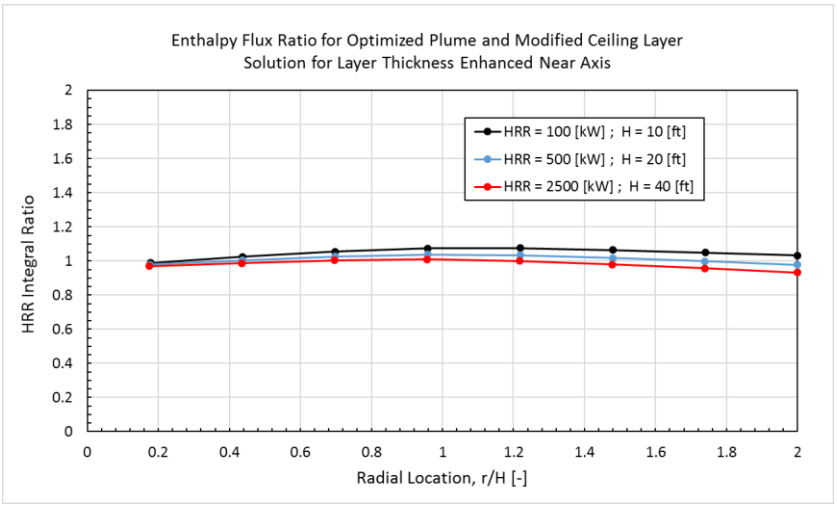

Figure 3-11: Ratio of Enthalpy Flux in the Ceiling Layer to the Convective Heat Release Rate of the Source Fire (optimized plume and modified ceiling layer with temperature correction at small radii). Peak Temperature Rise at the Ceiling Center, $\Delta T_{0,H}$: a. ~625°C (1,125°F); b. ~215°C (390°F); c. ~85°C (150°F).

A possible solution is to include a temperature dependent term that will increase the thickness of the layer at small radii, such as in the following formulation:

$$\ell_T / H_0 = 0.11 \cdot \left[1 + 1.5 \frac{T_{0,H}}{T_\infty} \exp\left(-6.4\, r / H_0\right) \right] \cdot \left[1 - \exp\left(-1.8\, r / H_0\right) \right] \quad . \qquad 3\text{-}54$$

The effect of this change is shown in Fig. 3-11. The enthalpy ratio at small radii is now significantly improved, taking the desired value of 1. However, an undesirable feature still remains, in the form of values for the enthalpy ratio about 15% too high at larger radii and high excess temperatures (plot a. in the figure). This residual discrepancy is considered acceptable and no additional effort has been expended to correct it. In conclusion, the set of equations presented above is considered to provide a fair representation of the flow in the ceiling layer.

Though not applicable to the cases in Fig. 3-11, which did not include the situation where the flame impinges on the ceiling, the following change is made to Eq. 3-40 to generalize it to those conditions:

$$r_{tr} = 0.162 \cdot \left(\frac{T_{0,H}}{T_\infty} \right)^{1/3} \left(H - z_0 \right) + z_{\lim} - H \qquad \text{for } z_{lim} > H \quad . \qquad 3\text{-}55$$

The above formulation is based on research by Heskestad and Hamada [10], who studied ceiling layers produced by flames with ratios of free flame height (no ceiling present) to ceiling height in the range 0.3 to 3. They found that, in the case where most heat release took place in the plume below the ceiling, the temperature data at various distances in the ceiling layer were properly scaled by the temperature rise on the plume axis and the plume width at the ceiling. However, the ceiling temperature data from flames under the lowest ceiling were displaced towards larger radii relative to the correlation referred to above. Another observation from Ref. [10] is that the flame extension under the ceiling was approximately equal to the length by which the flame would have extended above the ceiling, had the ceiling not been there.

4. Turning Region Extensions

4.1 Case of Small Temperature Differences

The relationships introduced in the previous sections apply to the portion of the ceiling layer beyond the turning region ($r > r_{tr}$). It is useful to extend those expressions to the flow closer to the axis of the plume, since practical applications may require consideration of locations in this turning region. The sought relationships are intended to provide a smooth transition from the vertical flow in the fire plume to the horizontal one in the ceiling layer.

The extension of the ceiling layer profiles to smaller radii can be achieved by approximately enforcing conservation of energy. Since the peak values of excess temperature, ΔT_m, and horizontal velocity, u_m, have been set equal to $\Delta T_{0,H}$ and $u_{0,H}$ at $r = r_{tr}$, it is reasonable to assume that these peak values will remain constant in the turning region. If the enthalpy flux is to be preserved, the only parameter left for potential modification is the depth of the layer. Given that the enthalpy flux depends linearly on radius, a possible adjustment is to make the depth of the layer inside the turning region inversely proportional to radius.

From the perspective of the thermal plume, a vertical profile at a given radius can be calculated from the standard correlations neglecting all possible effects due to the presence of the ceiling. At any radial cross section, two vertical profiles can therefore be calculated: one is from the plume equations and the other from the inward extrapolation of the ceiling layer correlation in the fashion indicated above. These two profiles can then be combined to extract the desired variation for the turning region.

This approach will be explored here by focusing on the excess temperature profile and by considering the half Gaussian portion only, i.e., neglecting the sub-layer.

4.1.1 Ceiling Layer

At the end of the turning region, the vertical temperature distribution is given by Eq. 3-46, namely:

$$\Delta T = \Delta T_{0,H} \exp\left[-\left(\frac{y}{\ell_{T,tr}} \right)^2 \right] \quad , \tag{4-1}$$

where $\ell_{T,tr}$ is given by Eq. 3-53 for $r = r_{tr} = 1.5\, b_{U,H}$. In the limit of small temperature differences, it is:

$$r_{tr} = 1.5 \cdot 0.108 \cdot H_0 = 0.162 \cdot H_0 \quad . \tag{4-2}$$

Substitution into Eq. 3-53 leads to the following expression for the depth of the layer, $\ell_{T,tr}$, at the end of the turning region:

$$\ell_{T,tr} / H_0 = 0.11 \cdot \left[1 + 1.5 \exp\left(-6.4 \cdot 0.162\right)\right] \cdot \left[1 - \exp\left(-1.8 \cdot 0.162\right)\right] = 0.04262 \quad . \tag{4-3}$$

If it is assumed that, inside the turning region, ℓ_T is inversely proportional to radius, i.e.:

$$\ell_T = \ell_{T,tr}\ r_{tr}/r \quad , \tag{4-4}$$

and that the temperature rise at the ceiling remains constant at $\Delta T_{0,H}$, then the normalized excess temperature profile in the ceiling layer as a function of radius, *r*, and distance from the ceiling, *y*, can be expressed as:

$$\Delta T_{CL}^{*} = \frac{\Delta T}{\Delta T_{0,H}} = \exp\left[-\left(\frac{y/H_0}{0.04262 \cdot 0.162\ H_0/r}\right)^2\right] \quad \text{for } r / r_{tr} \le 1 \quad . \tag{4-5}$$

Beyond the end of the turning region, the excess temperature decays in accordance with Eq. 3-44 and ℓ_T is still given by Eq. 3-53 yielding:

$$\Delta T_{CL}^{*} = \frac{\Delta T}{\Delta T_{0,H}} = \left(\frac{r}{r_{tr}}\right)^{-2/3} \exp\left[-\left(\frac{y}{\ell_T}\right)^2\right] \qquad \text{for } r / r_{tr} > 1 \quad . \tag{4-6}$$

4.1.2 Fire Plume

The temperature profile in the fire plume is given by Eq. 2-14, i.e.:

$$\Delta T\ = \Delta T_0\ \exp(-0.6931\ (r/b_T)^2) \quad , \tag{4-7}$$

where b_T is given by Eqs. 2-12 and 2-13 with $\alpha = 0.92$. After substitution of $H - y$ for *z*, the expression for b_T becomes:

$$b_T = \alpha \cdot 0.108 \cdot (H_0 - y) \quad . \tag{4-8}$$

In the non-reacting portion of the plume, the centerline excess temperature, ΔT_0, can be expressed in terms of distance from the ceiling as:

$$\frac{\Delta T_0}{\Delta T_{0,H}} = \left(1 - \frac{y}{H_0}\right)^{-5/3} \quad . \tag{4-9}$$

Substitution of Eqs. 4-8 and 4-9 into Eq. 4-7 yields the expression for excess temperature in the fire plume as a function of radius, *r*, and distance from the ceiling, *y*:

$$\Delta T_{FP}^{*} = \frac{\Delta T}{\Delta T_{0,H}} = \left(1 - \frac{y}{H_0}\right)^{-5/3} \exp\left[-0.6931\left(\frac{r/H_0}{\alpha \cdot 0.108 \cdot (1 - y/H_0)}\right)^2\right] \quad . \tag{4-10}$$

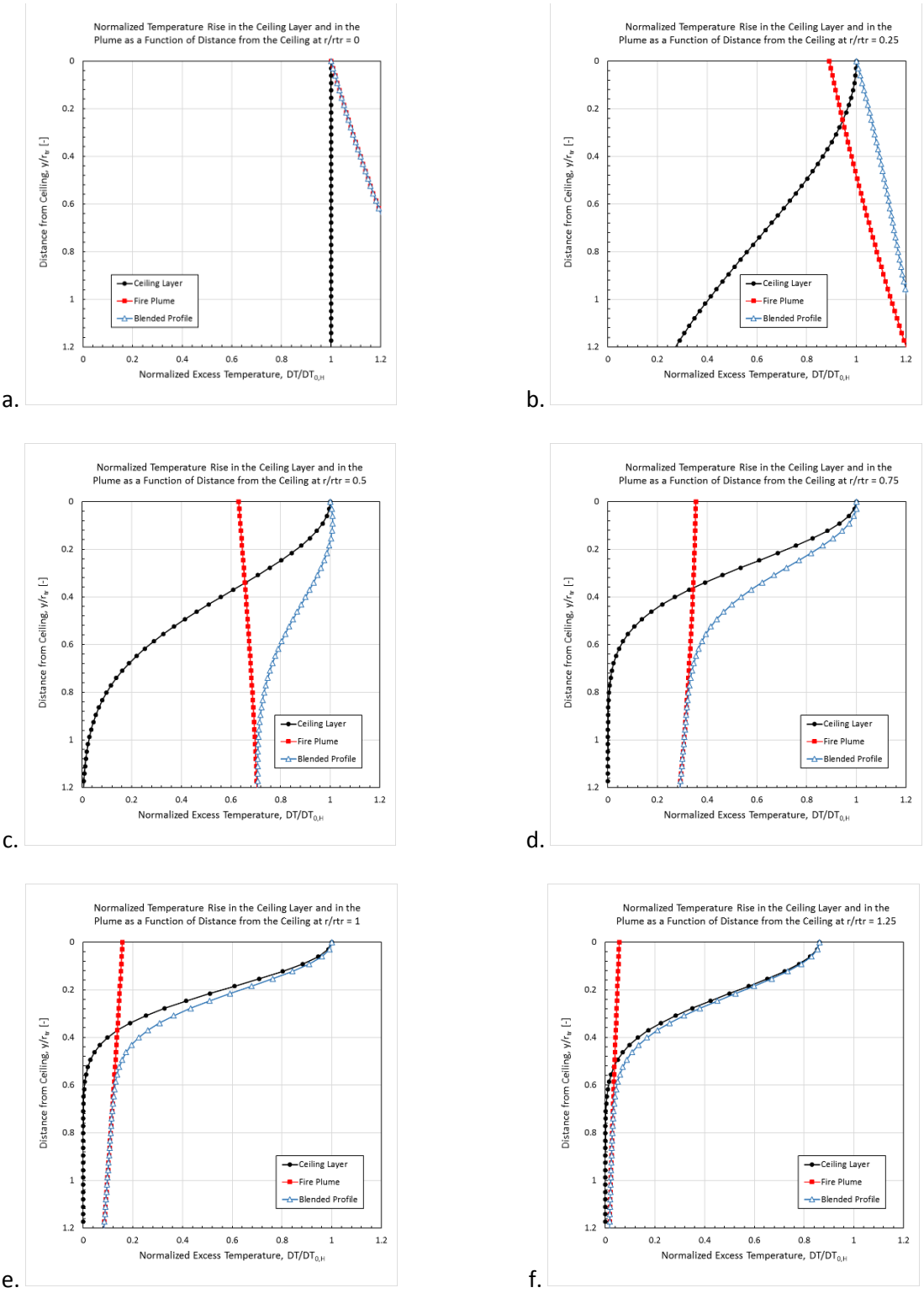

Figure 4-1: Normalized Temperature Rise in the Turning Region at Different Radial Locations, r/r_{tr} (a. =0; b. =0.25; c. =0.5; d. =0.75; e. =1.0; f. =1.25). Case of Negligible Temperature Differences and $r_{tr} = 1.5\ b_{u,H}$.

4.1.3 Merging of Fire Plume and Ceiling Layer Formulas

At any radius, *r*, Eqs. 4-10 and 4-6 describe the vertical variation of excess temperature respectively from the perspective of the unconfined fire plume and from the inwardly extrapolated ceiling layer. These two profiles will now be used as the basis for the selection of a temperature distribution for the turning region by forcing a smooth transition from the fire plume profile on the plume axis to the ceiling layer profile at large radii. The formulation selected to achieve this result is:

$$\Delta T^* = \Delta T^*_{FP} + \gamma\, \Delta T^*_{CL} \quad , \tag{4-11}$$

where

$$\gamma = 1 - \frac{\Delta T^*_{FP,0}}{\Delta T^*_{CL,0}} \exp\left(-\frac{r}{r_{tr}} \frac{y}{r_{tr}} \frac{\ell_{T,tr}}{\ell_T} \right) \quad . \tag{4-12}$$

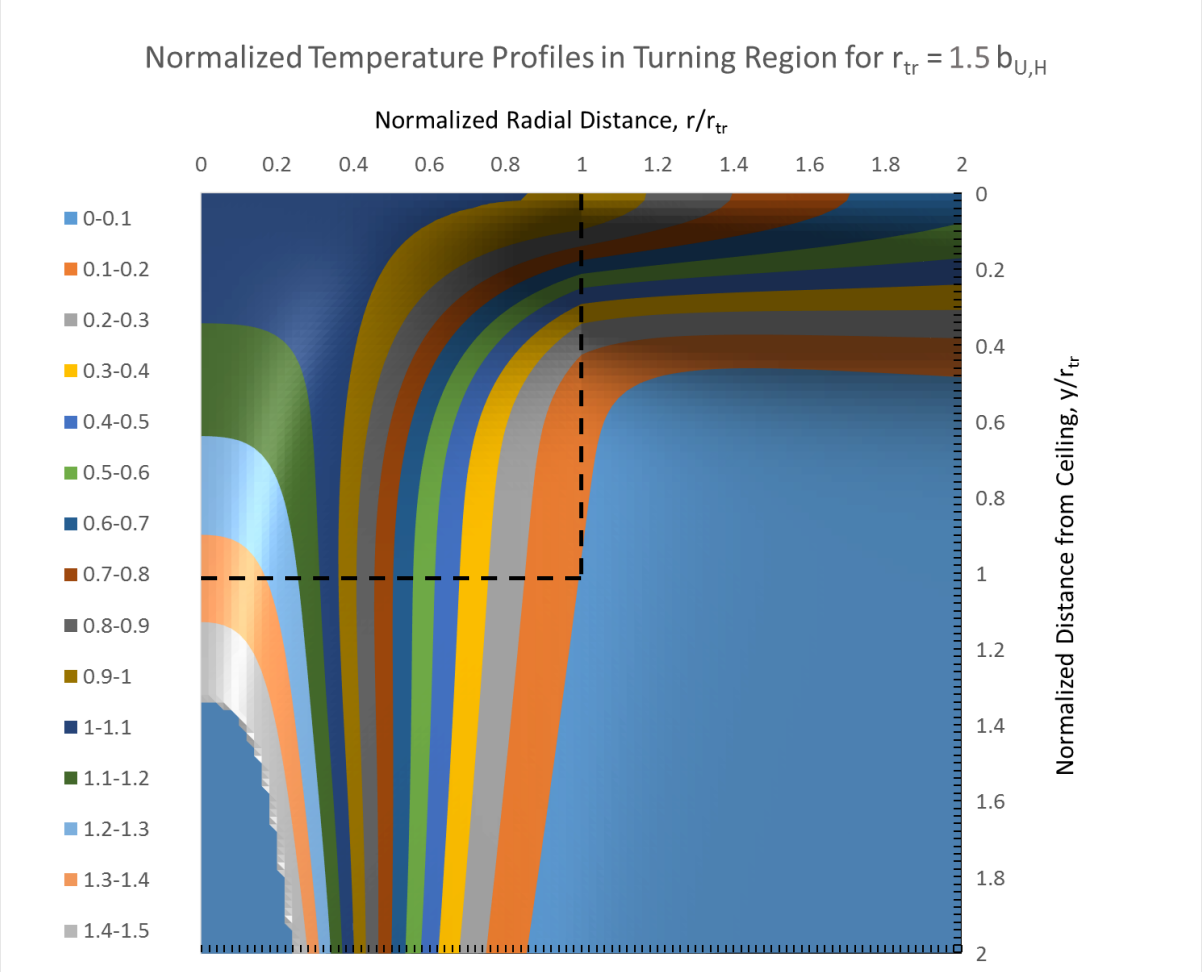

Figure 4-2: Contours of Normalized Temperature Rise in the Turning Region of a Fire Plume Transitioning to a Ceiling Layer. Case of Negligible Temperature Differences and $r_{tr} = 1.5\ b_{u,H}$.

In Eq. 4-12, the two quantities $\Delta T^*_{FP,0}$ and $\Delta T^*_{CL,0}$ refer to the values of ΔT^*_{FP} and ΔT^*_{CL} at radius, *r*, and at *y* = 0, i.e., at the ceiling. The effect achieved by the implementation of the algorithm in Eqs. 4-11 and 4-12 is demonstrated by the examples shown in Fig. 4-1. The six plots in the figure present the vertical profiles at a constant value of r/r_{tr}. Taking plot "e" as an example (corresponding to the nominal exit from the turning region, r/r_{tr} = 1.0), the black curve with solid circles shows the temperature profile in the ceiling layer in the absence of the fire plume. Similarly, the red curve with solid squares is for the temperature distribution in the fire plume in the absence of the ceiling layer. The result of blending these two curves is represented by the blue line with the open triangles.

As can be seen in the other plots, as r/r_{tr} decreases, the depth of the ceiling layer profile increases and the fire plume profile takes on higher values. The blended profile for the normalized temperature ratio, ΔT^*, at the ceiling always starts from a value of 1 within the turning region, owing to the normalization of temperatures by $\Delta T_{0,H}$, and from a lower value outside of that region (see plot "f"), accounting for the radial decay in the ceiling layer. In all cases, the blended profile merges with the fire plume profile at large distances from the ceiling. The resulting two-dimensional distribution in the turning region is illustrated by the contour plot in Fig. 4-2.

The same exercise, when applied to the formulas for the variation of vertical velocity in the fire plume and horizontal velocity in the ceiling layer (cf. Section A.3.2 of Appendix A), yields the result for the normalized scalar velocity field shown in Fig. 4-3. These profiles are wider in the plume region and thinner in the ceiling layer than those in Fig. 4-2 for the temperature field, reflecting the fact that $b_T = \alpha\, b_U$ with α = 0.92 in the plume (cf. Eq. 2-13) and $\ell_U = 0.8 \cdot \ell_T$ in the ceiling layer (cf. Eq. 3-43). The contours in the turning region, nominally identified by the dashed lines, provide a somewhat arbitrary, but realistic representation of the zone of transition between the two flows.

4.2 Case of Arbitrary Temperature Rise

The simplified case of small temperature differences presented in the previous section has supported the development of a formalism that smoothly describes the flow transition from the vertical fire plume to the horizontal ceiling layer. However, the case of more practical interest is where large temperature differences are present. In that case, a unified description is no longer possible, and the value of the temperature rise on the fire plume axis at the ceiling, $\Delta T_{0,H}/T_\infty$, becomes a parameter. Furthermore, as the value of this parameter approaches 3.5 (cf. Eqs. 2-1 and 2-2), different forms of the correlations need to be considered to account for the transition from the non-reacting to the reacting portion of the fire plume. This more general problem is addressed next for the case where there is no flame impingement on the ceiling, i.e., $\Delta T_{0,H}/T_\infty < 3.5$.

4.2.1 Ceiling Layer

The equations introduced in the previous section for the case of negligible temperature increases remain valid with the following exceptions. More specifically, Eq. 4-1 still describes the vertical excess temperature variation at the end of the turning region, but the transition radius is now given by:

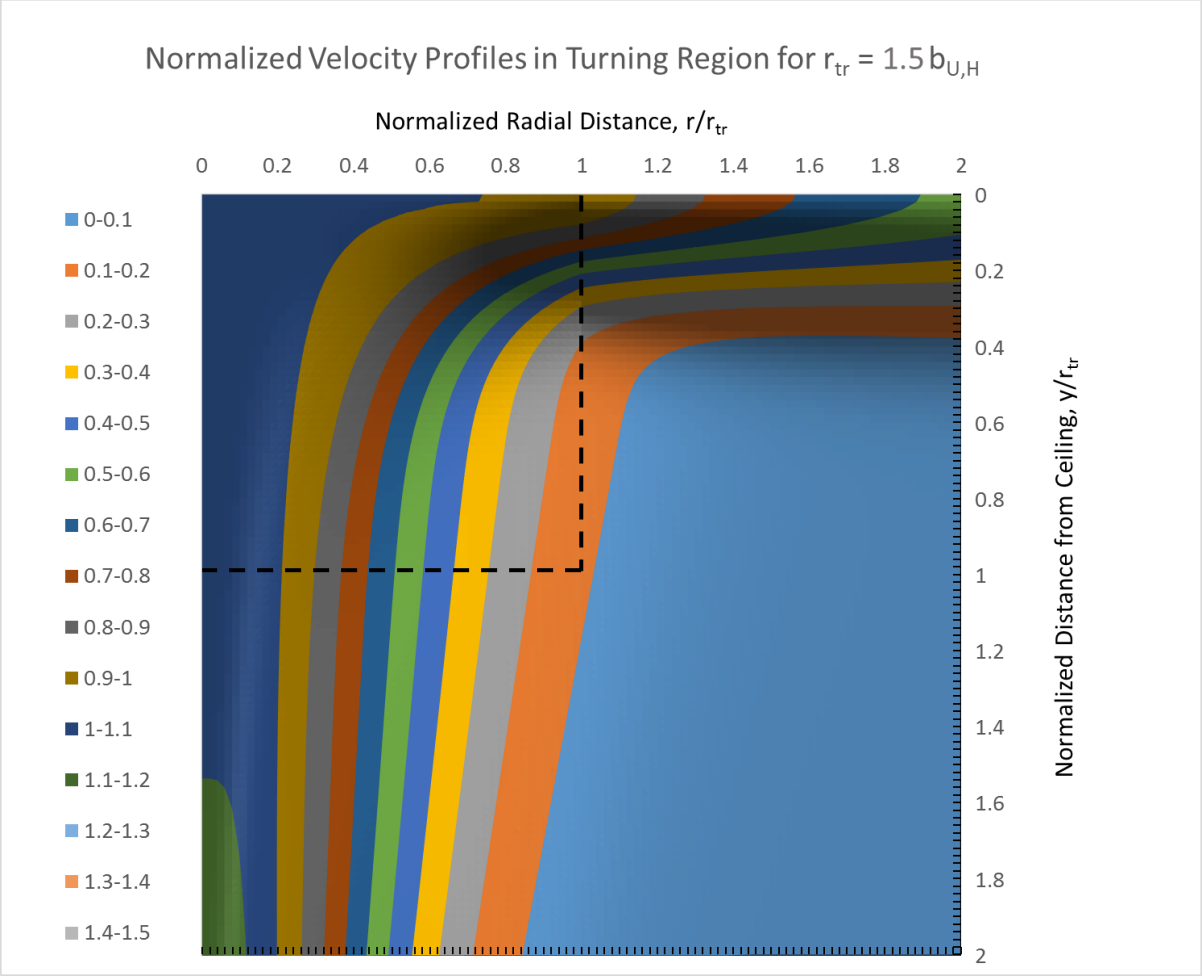

Figure 4-3: Contours of Normalized Scalar Velocity Field in the Turning Region of a Fire Plume Transitioning to a Ceiling Layer. Case of Negligible Temperature Differences and r_{tr} = 1.5 $b_{u,H}$.

$$r_{tr} = 0.162 \cdot \left(1 + \frac{\Delta T_{0,H}}{T_\infty}\right)^{1/3} H_0 + MAX\,(0,\, z_{\lim} - H) \quad . \tag{4-13}$$

The depth of the layer, $\ell_{T,tr}$, at the end of the turning region now is (cf. Eq. 3-54):

$$\ell_{T,tr} / H_0 = 0.11 \cdot \left[1 + 1.5 \cdot \left(1 + \frac{\Delta T_{0,H}}{T_\infty}\right) \exp\left(-6.4\, \frac{r_{tr}}{H_0}\right)\right] \cdot \left[1 - \exp\left(-1.8 \cdot \frac{r_{tr}}{H_0}\right)\right] \quad , \tag{4-14}$$

where r_{tr}/H_0 is given by Eq. 4-13. Inside the turning region, ℓ_T is still taken to be inversely proportional to radius as per Eq. 4-4. Given that the temperature rise at the ceiling in this region is assumed to remain constant at $\Delta T_{0,H}$, the normalized excess temperature profile in the ceiling layer as a function of radius, r, and distance from the ceiling, y, can be expressed as:

$$\Delta T_{CL}^{*} = \frac{\Delta T_{CL}}{\Delta T_{0,H}} = \exp\left[-\left(\frac{y/H_0}{\ell_{T,tr}/H_0 \cdot r_{tr}/r} \right)^2 \right] \qquad \text{for } r / r_{tr} \le 1 \quad . \qquad 4\text{-}15$$

Beyond the end of the turning region, the excess temperature decays in accordance with Eq. 3-44 and ℓ_T is now given by Eq. 3-54 yielding:

$$\Delta T_{CL}^{*} = \frac{\Delta T_{CL}}{\Delta T_{0,H}} = \left(\frac{r}{r_{tr}} \right)^{-2/3} \exp\left[-\left(\frac{y/H_0}{\ell_T/H_0} \right)^2 \right] \qquad \text{for } r / r_{tr} > 1 \quad . \qquad 4\text{-}16$$

It can be noted that all of the above expressions depend on normalized variables (r/H_0, y/H_0 and r_{tr}/H_0) and that the temperature ratio $\Delta T_{0,H}/T_\infty$ is one additional parameter in the expressions for r_{tr} and $\ell_{T,tr}$.

4.2.2 Fire Plume

The same situation mentioned in connection with the ceiling layer is present in the extension of the fire plume equations to the case of finite temperature rise. For example, the temperature profile in the fire plume is still given by Eq. 4-7, but now b_T is given by an expression, which includes the temperature rise at the ceiling:

$$b_T = \alpha \cdot 0.108 \cdot \left(1 + \frac{\Delta T_{0,H}}{T_\infty} \right)^{1/3} \left(H_0 - y \right) \qquad . \qquad 4\text{-}17$$

One last adjustment is needed to identify the separation between the non-reacting and reacting portions of the fire plume. Equation 4-9 for the centerline excess temperature, ΔT_0, remains valid in the non-reacting portion of the plume, i.e., for as long as $\Delta T_0/T_\infty \le 3.5$ (cf. Eq. 2-1 and 2-2). If the flame is not impinging on the ceiling ($\Delta T_{0,H}/T_\infty \le 3.5$), Eq. 4-9 provides an expression for the distance, y_{lim}, below the ceiling at which the transition to the reacting portion of the plume takes place:

$$\frac{y_{\lim}}{H_0} = 1 - \left(\frac{1}{3.5} \frac{\Delta T_{0,H}}{T_\infty} \right)^{3/5} \qquad . \qquad 4\text{-}18$$

This results in the following expressions for excess temperature on the fire plume axis as a function of distance from the ceiling, y:

$$\begin{aligned} &\frac{\Delta T_0}{T_\infty} = \frac{\Delta T_{0,H}}{T_\infty} \left(1 - \frac{y}{H_0} \right)^{-5/3} && \text{for } y < y_{lim} \\ &\frac{\Delta T_0}{T_\infty} = 3.5 && \text{for } y \ge y_{lim} \quad . \end{aligned} \qquad 4\text{-}19$$

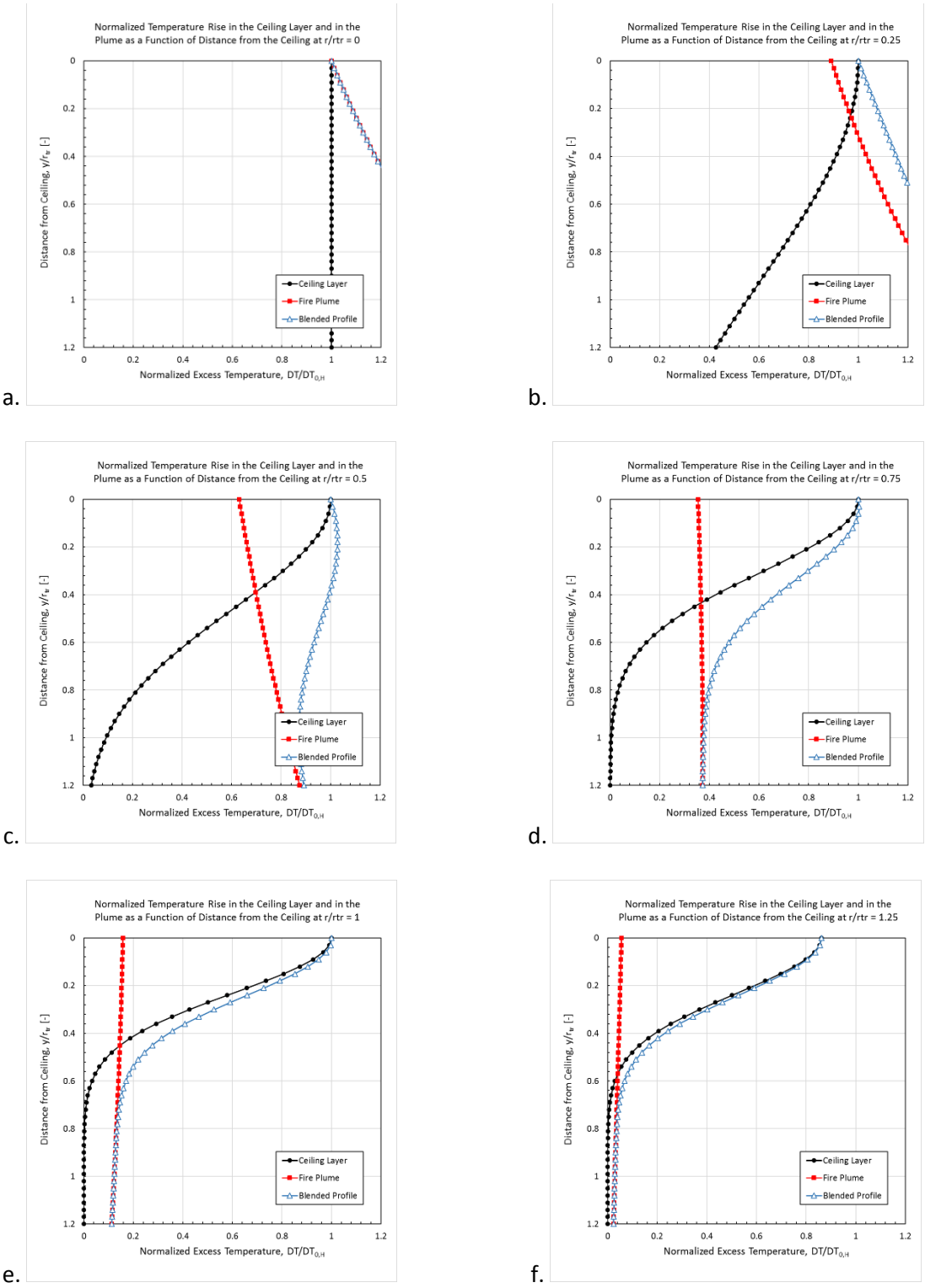

Figure 4-4: Normalized Temperature Rise in the Turning Region at Different Radial Locations, r/r_{tr} (a. =0; b. =0.25; c. =0.5; d. =0.75; e. =1.0; f. =1.25). Case of Temperature Rise at Ceiling Center of $\Delta T_{0,H}/T_{\infty} = 2$ and $r_{tr} = 1.5\ b_{u,H}$.

Finally, the expression for excess temperature in the fire plume as a function of both radius, *r*, and distance from the ceiling, *y*, becomes:

$$\Delta T_{FP}^{*} = \frac{\Delta T_{FP}}{\Delta T_{0,H}} = \frac{\Delta T_0 / T_\infty}{\Delta T_{0,H} / T_\infty} \exp\left[-0.6931 \left(\frac{r/H_0}{\alpha \cdot 0.108 \cdot (1 + \Delta T_0 / T_\infty)^{1/3} \cdot (1 - y/H_0)} \right)^2 \right] \quad \text{4-20}$$

Similar to the case of the ceiling layer equations, the normalized temperature rise in the fire plume is only a function of r/H_0, y/H_0 and the temperature ratio $\Delta T_{0,H}/T_\infty$.

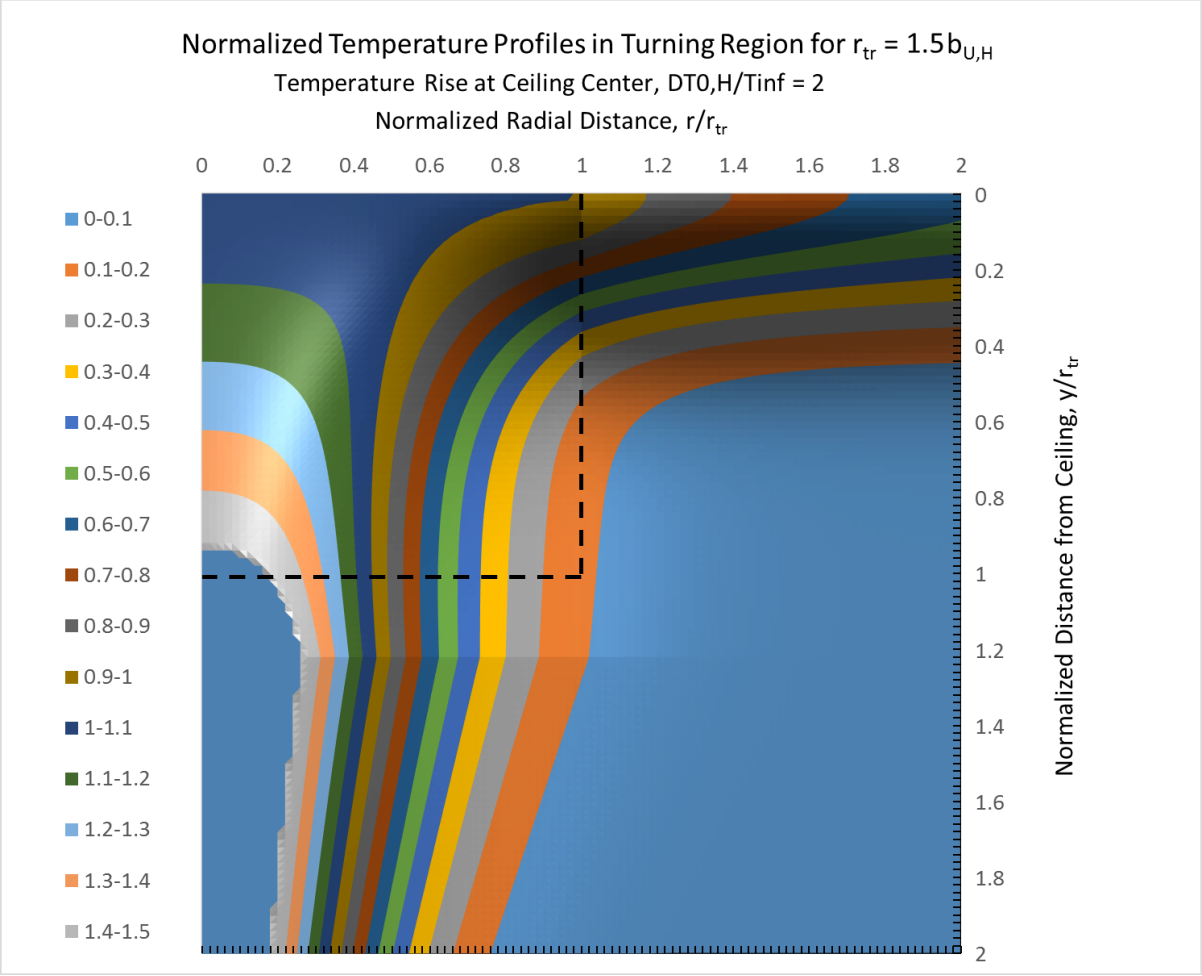

Figure 4-5: Contours of Normalized Temperature Rise in the Turning Region of a Fire Plume Transitioning to a Ceiling Layer. Case of Temperature Rise at Ceiling Center of $\Delta T_{0,H}/T_\infty = 2$ and $r_{tr} = 1.5\ b_{u,H}$.

4.2.3 Merging of Fire Plume and Ceiling Layer Formulas

The merging of the fire plume with the ceiling layer is done using the same formulation introduced for the case of negligible temperature rise, i.e., Eqs. 4-11 and 4-12. The result for the case of $\Delta T_{0,H}/T_\infty = 2$ is presented in Fig. 4-4 as a series of six sets of vertical profiles at the same constant values of r/r_{tr} used for the plots in Fig. 4-1.

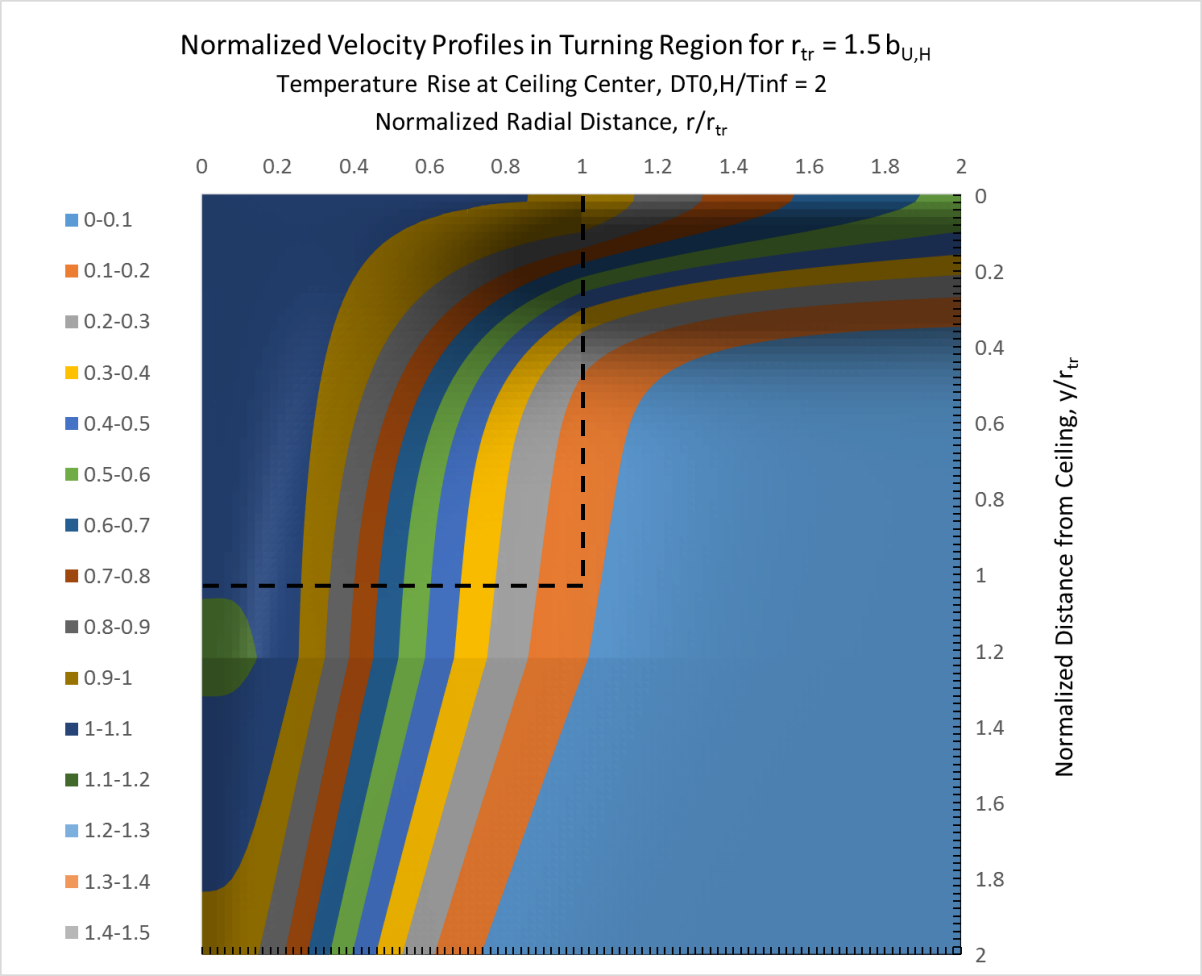

Figure 4-6: Contours of Normalized Scalar Velocity Field in the Turning Region of a Fire Plume Transitioning to a Ceiling Layer. Case of Temperature Rise at Ceiling Center of $\Delta T_{0,H}/T_\infty = 2$ and $r_{tr} = 1.5\ b_{u,H}$.

Close comparison with the plots of Fig. 4-1 shows general similarities but significant quantitative differences. Even in the normalized scales used in the plots, excess temperatures are higher and the profiles are deeper than in the case of negligible temperature differences. These differences are further emphasized by the contour plot in Fig. 4-5. A feature of these contours is the trend discontinuity at about $y/r_{tr} = 1.2$, which corresponds to the end of the non-reacting portion of the plume. Comparison with the analogous plot for $\Delta T_{0,H}/T_\infty << 1$ of Fig. 4-2 shows the profiles to be somewhat wider around the turning region. However, conclusions based on scaled variables are not easy to reach, since the

contours in Fig. 4-5 represent higher values of excess temperature than the corresponding ones in Fig. 4-2.

A similar contour plot can be developed for the normalized scalar velocity field, by considering the formulas for the variation of vertical velocity in the fire plume and horizontal velocity in the ceiling layer (cf. Section A.3.2 of Appendix A). It is shown in Fig. 4-6. As in the case of the temperature contours in Fig. 4-5, there is a horizontal discontinuity at the point of transition from the flame to the non-reacting plume.

Comparison with the plot for $\Delta T_{0,H}/T_\infty << 1$ of Fig. 4-3 prompts comments similar to those made in connection with the temperature data. In the case of the velocity, the variation in the flame region is by square root of height. In other words, moving down from the ceiling, the velocity on the plume axis first increases by 1/3 power of distance, reaches a maximum at the non-reacting/reacting interface and then decreases. This explains the area of high values at around $y/r_{tr} = 1.2$ and $r/r_{tr} = 0$-0.1. It is also interesting to note that, here again, $\Delta T_{0,H}/T_\infty$ is the only parameter, though the value of the normalizing velocity, $u_{0,H}$, is a function of H_0.

Appendix A contains a complete summary of the formulas describing the fire plume, the ceiling layer, and the turning region.

One final comment concerns the extent of the ceiling layer over which the above interpolation procedure should be applied. Because of the rapid radial decay of the fire plume profiles (cf. Eqs. 2-14 and 2-15), their contribution vanishes at sufficiently large values of the r/r_{tr} ratio. In practice, such a contribution can be neglected for $r/r_{tr} > 2$-2.5. Also, the contribution from the ceiling layer values can be neglected at locations close to the axis, as defined by $r/r_{tr} \leq 0.01$. In conclusion, the interpolation procedure is only applied in the range $0.01 < r/r_{tr} < 2.5$.

5. Comparisons with Experimental Data

The reformulated equations will now be tested by comparison with data from well-controlled pool fires. The revised fire plume and ceiling layer correlations have been implemented in the TarResponse program (V2.2.1). The main output of this program consists of sprinkler link temperatures predicted from the values of gas temperatures, which are normally measured at a distance of 6 in. (0.15 m) down from the ceiling. An additional output is in the form of estimates of convective heat release rate (HRR) of the fire. These estimates are provided individually for each of five groups, in which the thermocouples are about equally divided on the basis of distance from the axis of the fire (Group #1 @ 0-18 ft, #2 @ 18-27 ft, #3 @ 27-34 ft, #4 @ 34-40 ft, #3 @ 40-50 ft). The degree to which the HRR predictions from the various groups show consistency is taken as a measure of model validation.

5.1 Heptane Pool – 44-in. Diameter under 23.4-ft Ceiling

The estimates from the five zones for the convective HRR of this small pool, made using the original correlations of the KYS model, are shown in Fig. 5-1. Also shown in the figure as the solid black line is an estimate of the convective HRR based on load cell measurements of fuel consumption rate. As was noted before, there is a large discrepancy among the values estimated by the different groups of thermocouples, with the greatest departure being associated with the TCs in Zone 5 (HRR_Avg5 curve in Fig. 5-1).

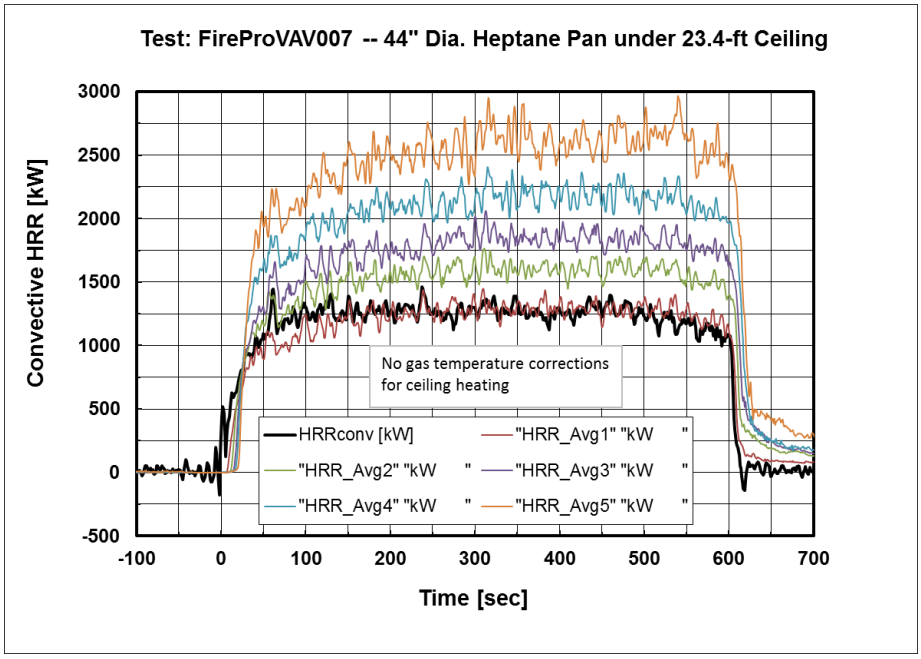

Figure 5-1: Average Net Convective Heat Release Rate from Each of the Five TC Groups for a Test with a 44-in. Heptane Pool Fire. Predictions based on KYS Model. Lowest Curve is for Group 1, Highest for Group 5.

The same HRR estimates made with the model presented here are shown in Fig. 5-2. The spread among the different curves is now practically eliminated. This result is taken as validation of the selection of the decay formula for the ceiling layer temperature (cf. Eq. 3-44).

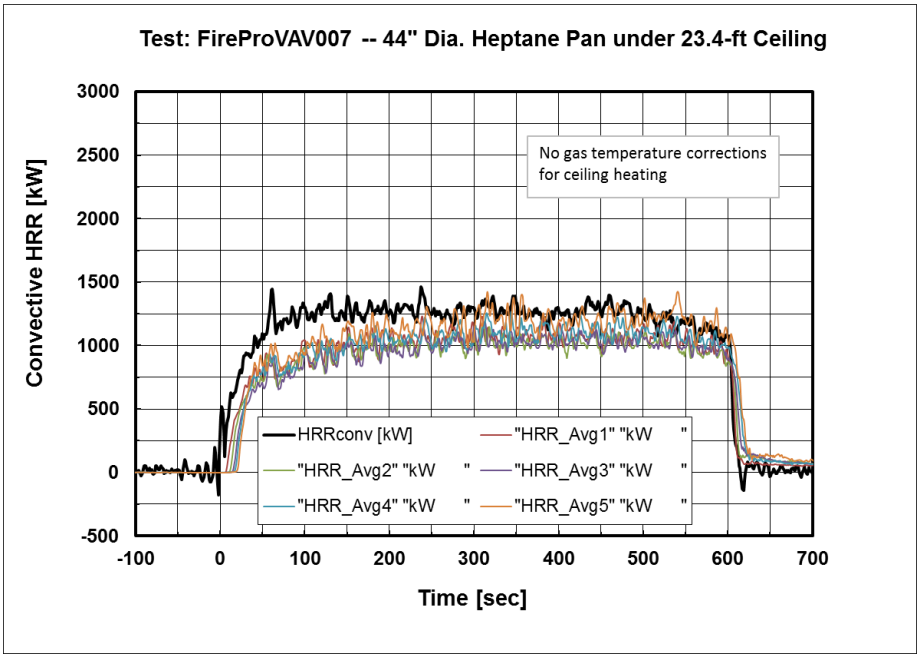

Figure 5-2: Average Net Convective Heat Release Rate from Each of the Five TC Groups for a Test with a 44-in. Heptane Pool Fire. Predictions Based on Present Model without Data Correction.

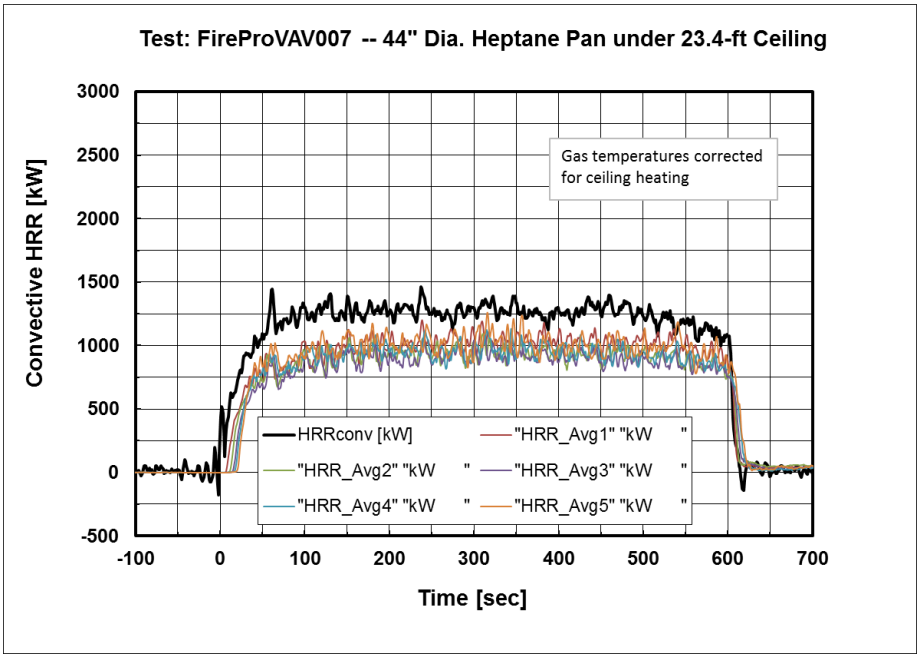

Figure 5-3: Average Net Convective Heat Release Rate from Each of the Five TC Groups for a Test with a 44-in. Heptane Pool Fire. Predictions Based on Present Model after Data Correction to Account for Ceiling Heating.

Finally, if the estimates are repeated after correcting the data for effects associated with the heating of the ceiling using Eq. 3-31, the result is as shown in Fig. 5-3. The predictions from the different zones remain clustered and are now somewhat lower than the convective HRR estimate based on the load cell data.

5.2 Heptane Pool – 9x9 ft under 49-ft Ceiling

A more challenging test of the correlations is provided by the data obtained with a larger pool. In this case, the size of the pan is 9 ft by 9 ft (2.74 m by 2.74 m) and the ceiling is at 49 ft (14.9 m). These conditions provide a particularly severe test for the method being evaluated here, because of the high ceiling temperatures generated by the fire over a sustained period of time. Convective HRR estimates based on the previous KYS method are shown in Fig. 5-4. There is significant spread among the results from the five zones, with the data from Zone 1 (within 18 ft (5.5 m) of the fire plume axis) yielding a steady-state value of convective HRR of about 17.5 MW. This value is in good agreement with an estimate based on a scaled extrapolation of the load cell measurements from the test with the 44-in. pool. The data from Zone 5 (TCs at radii between 40 ft (12 m) and 50 ft (15 m)) yield about 38 MW, and those from the other three zones are somewhere in between.

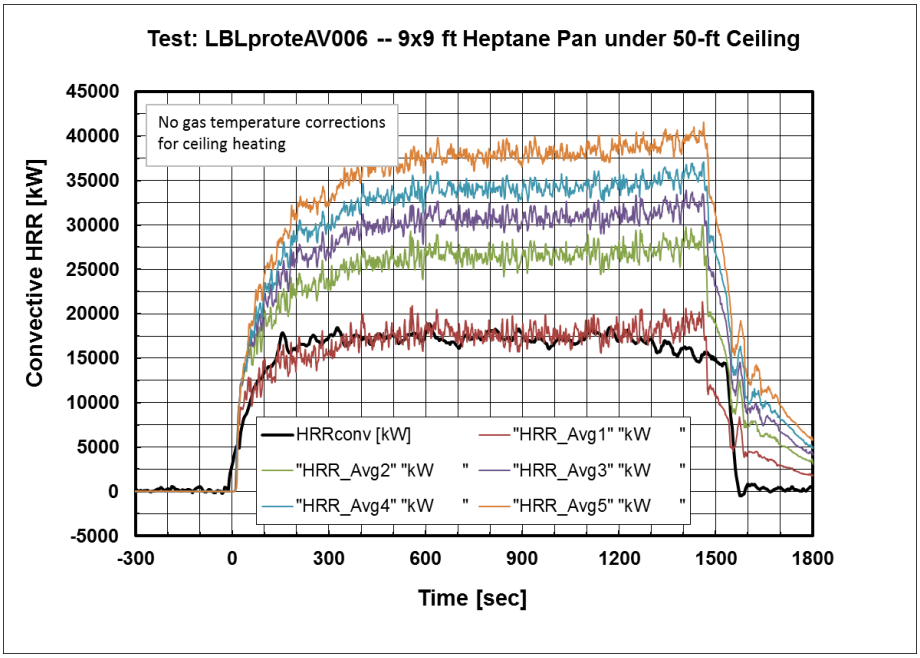

Figure 5-4: Average Net Convective Heat Release Rate from Each of the Five TC Groups for a Test with a 9x9 ft Heptane Pool Fire. Predictions based on KYS Model. Lowest Curve is for Group 1, Highest for Group 5.

The same estimates based on the present model are shown in Fig. 5-5. These predictions have less spread than those in Fig. 5-4 from the KYS model, with the estimate from Zone 5 reaching up to 30 MW instead of the 38 MW of that model. The spread among the various zones remains significant, however.

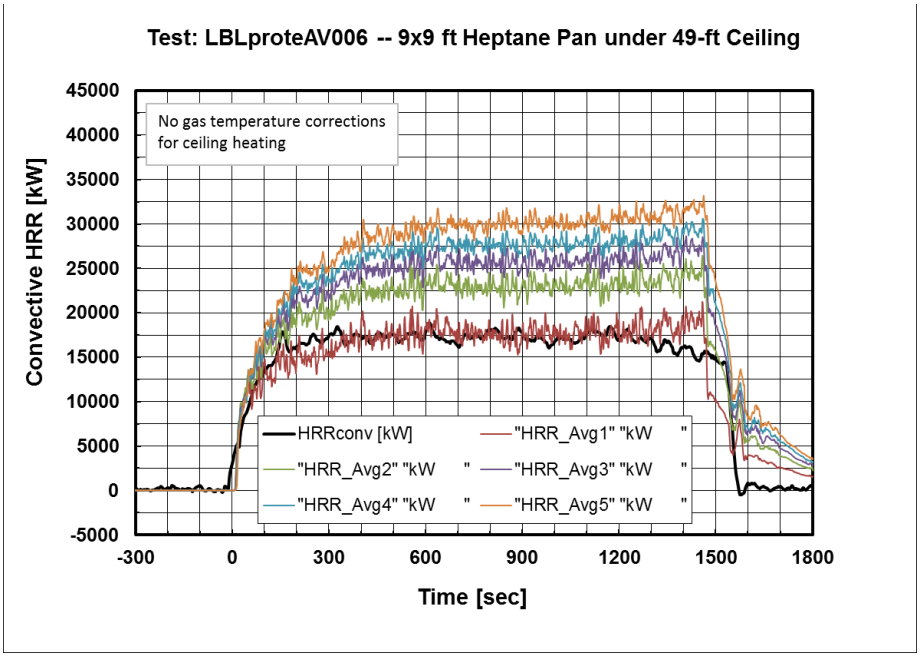

Figure 5-5: Average Net Convective Heat Release Rate from Each of the Five TC Groups for a Test with a 9x9 ft Heptane Pool Fire. Predictions Based on Present Model. Lowest Curve is for Group 1, Highest for Group 5.

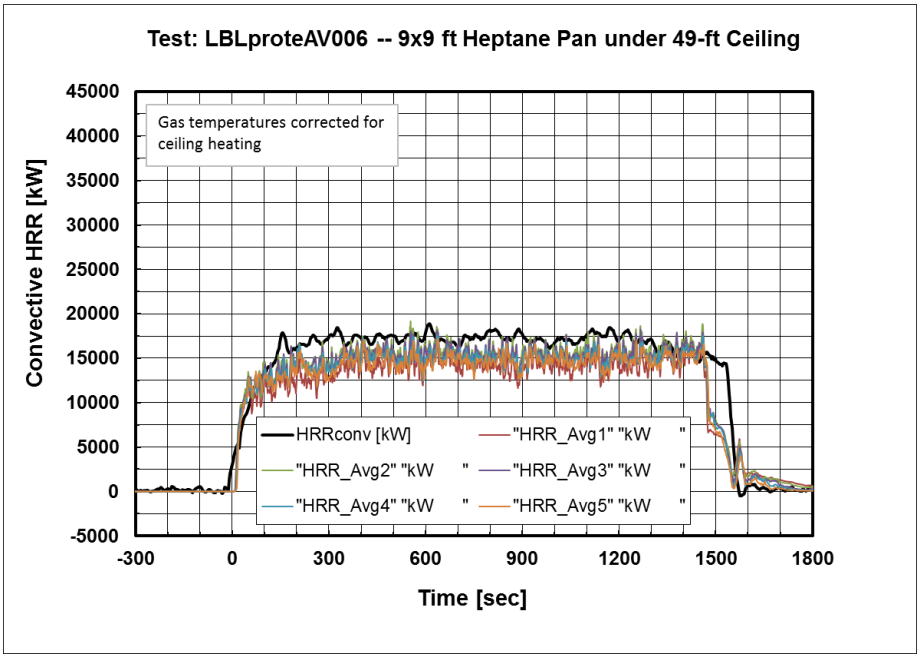

Figure 5-6: Average Net Convective Heat Release Rate from Each of the Five TC Groups for a Test with a 9x9 ft Heptane Pool Fire. Predictions Based on Present Model after Data Correction to Account for Ceiling Heating.

Finally, the predictions with the gas temperatures corrected using Eq. 3-31 are shown in Fig. 5-6. The profiles from the five zones have now collapsed onto one, though the predicted level of convective HRR is now around 15 MW, somewhat lower than the 17.5 MW from the extrapolated load cell measurements.

5.3 Heptane Pool – 7x7 ft under 49-ft Ceiling

The last case to be considered is that of a 7 ft by 7 ft (2.1 m by 2.1 m) heptane pool under a 49-ft (14.9-m) ceiling, which is presented through the same three sets of estimates used in the previous two examples. They are shown in Figs. 5-7 to 5-9 for the cases of the KYS model and the present model without temperature correction and the present model with temperature correction, respectively. The same pattern observed with the first two pools is essentially repeated here. Good consistency in the convective HRR predictions is achieved with the present model applied to corrected temperature data, though the average HRR of about 7.5 MW is somewhat lower than the estimate from extrapolated load cell measurements.

Overall, the present model predictions of convective HRR are validated by these comparisons with pool fire data. If anything, they point to the fact that there is a reduced need for the correction to account for heating of the ceiling.

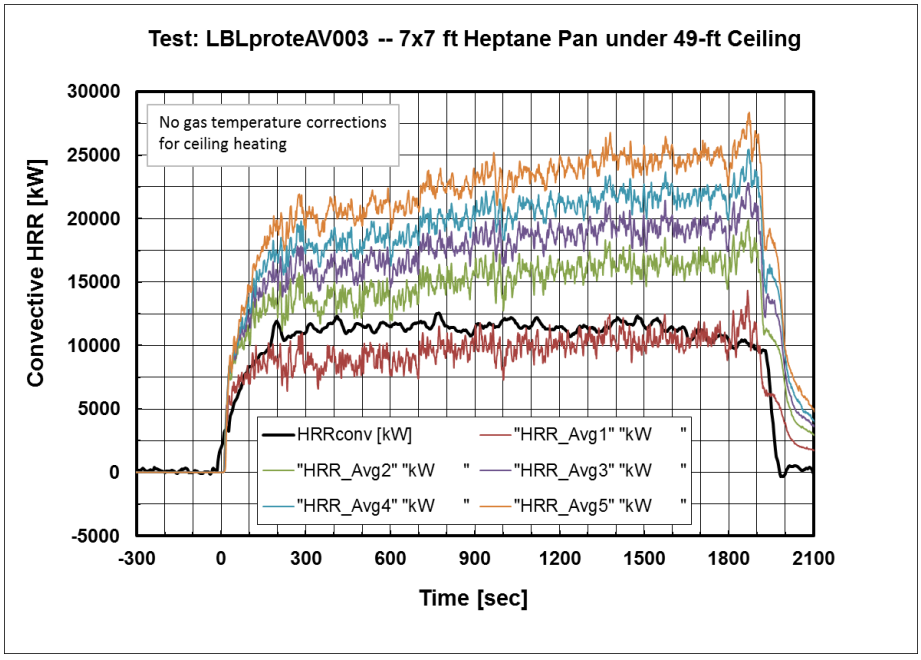

Figure 5-7: Average Net Convective Heat Release Rate from Each of the Five TC Groups for a Test with a 7x7 ft Heptane Pool Fire. Predictions based on KYS Model. Lowest Curve is for Group 1, Highest for Group 5.

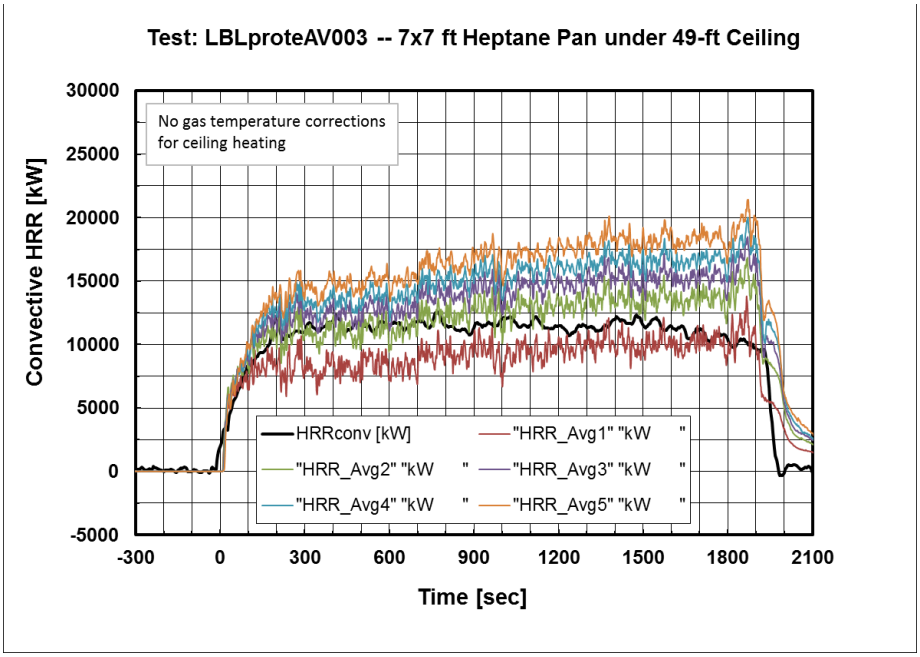

Figure 5-8: Average Net Convective Heat Release Rate from Each of the Five TC Groups for a Test with a 7x7 ft Heptane Pool Fire. Predictions Based on Present Model. Lowest Curve is for Group 1, Highest for Group 5.

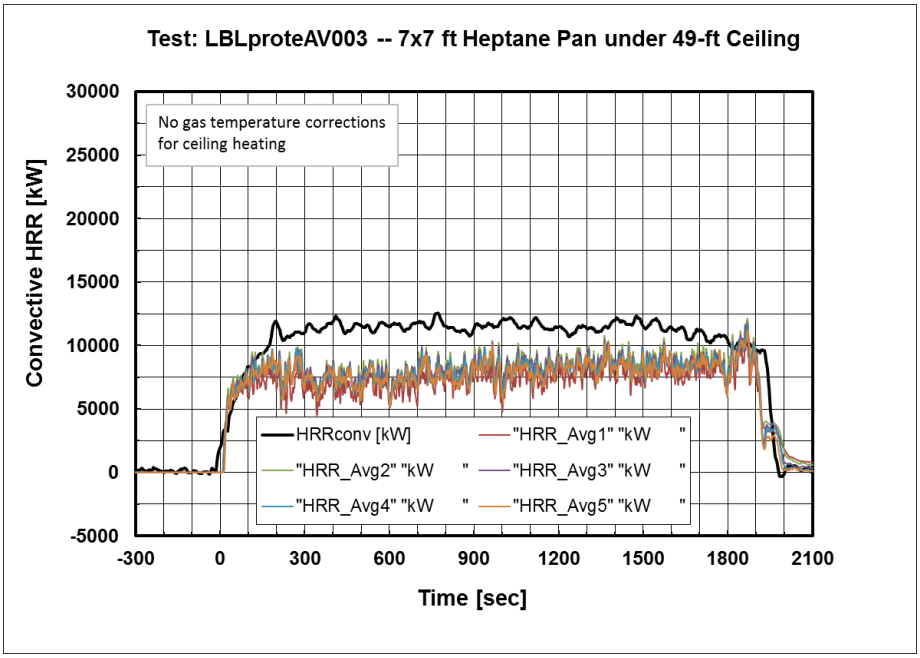

Figure 5-9: Average Net Convective Heat Release Rate from Each of the Five TC Groups for a Test with a 7x7 ft Heptane Pool Fire. Predictions Based on Present Model after Data Correction to Account for Ceiling Heating.

6. **Summary and Conclusions**

The work detailed in the report has undertaken the task to revisit the correlations for gas temperature and velocity in fire plumes and ceiling layers and to develop a formulation for the transition between the two. The driving motivation has come from the desire to improve the consistency and, possibly, accuracy of predictions of convective heat release rate (HRR) based on gas temperature measurements near the ceiling during fire tests.

The fire plume correlations have been evaluated for compliance with energy and momentum conservation. The analysis has resulted in small adjustments in some of the correlation constants, whose values still remain within the range of those reported in the literature. The practical impact of these changes is relatively modest.

The ceiling layer correlations have been critically analyzed using the calculated enthalpy flux as a figure of merit to guide their modification. The behavior of a correlation for the depth of the ceiling layer from the KYS model [4], which has been used up until now, has been the object of particular attention. The changes introduced for that quantity and for the temperature decay are believed to be responsible for a significant improvement in the consistency of the predictions of convective HRR obtained from measurements at different distances from the fire axis. Evidence of this outcome is provided by the reduced need to correct the gas temperature measurements to account for heating of the ceiling during long duration tests. In most sprinklered fire tests, such correction will, therefore, not be necessary.

The third and last aspect of the work addressed the question of a smooth transition between the fire plume and ceiling layer flows. Such a transition takes place in a turning region near the ceiling, which is not covered by the correlations. Its radial extent is estimated at about 1.5 times the fire plume half width at the ceiling. As an example, in the case of a fire with the ceiling at 20 ft (6.1 m) from the plume's virtual origin, the turning region radius is estimated to be about 3.3-4.0 ft (1.0-1.2 m). The formulation developed by this analysis is completely empirical. It does provide for the sought smooth transition and it can conceivably be used to estimate the orientation of the velocity vectors in this turning region. This last aspect, which may be the object of future work, would be useful in predicting first sprinkler activation in cases of under-one fire tests.

One desirable improvement needs to be implemented: the introduction of accounting for travel time from the fire to the point of measurement. This detail becomes important when predictions of fire growth rate are of interest in rapidly growing fires, since in that case differences in travel time skew the results, particularly if they are obtained from measurements far from the fire axis. Work on this issue is well underway and will be presented in an upcoming report.

Nomenclature

b_T half width of plume temperature profile [m]
b_U half width of plume velocity profile [m]
b_{CL} ceiling layer radial length scale [m]
c_p specific heat of gases [= 1000 J/kg K]
g acceleration of gravity [= 9.806 m/s^2]
H ceiling height [m]
H_0 ceiling height from elevation of virtual origin [m]
I integral value [-]
$\dot{m}$ mass flux [kg/s]
M molecular weight of air [= 29.1 kg/kg-mole]
p_∞ ambient pressure [= 1.01325·10^5 Pa]
$\dot{Q}^*$ normalized heat release rate [-]
$\dot{Q}_c$ convective heat release rate [kW]
$\dot{Q}_{ent}$ total enthalpy flux [kW]
r radial distance from plume axis [m]
r_{tr} radius of turning region [m]
R universal gas constant [= 8314 kg m^2/s^2 kg-mole K]
s factor in the formula for thermal depth of ceiling layer [-]
T temperature [K]
T_∞ ambient temperature [K]
u vertical velocity in the fire plume or horizontal velocity in ceiling layer [m/s]
u_0 peak vertical velocity in the fire plume [m/s]
u_m peak horizontal velocity in the ceiling layer [m/s]
u_m^* normalized peak horizontal velocity in the ceiling layer [-]
$u_{0,lim}$ value of vertical velocity u_0 at height z_{lim} [m/s]
$u_{0,H}$ maximum velocity in the fire plume at the ceiling [m/s]
$\dot{W}$ momentum flux [kg·m/s^2]
y distance from ceiling [m]
y_{lim} distance from ceiling of boundary between reacting and non-reacting plume regions [m]
z_0 elevation of the virtual origin above the fire source [m]
z vertical distance [m]
$z_{0,I}$ virtual origin elevation for zero heat release rate [m]
z_{lim} transition height between reacting and non-reacting plume regions [m]

Greek Symbols

α ratio between thermal and velocity layer depth [-]

δ laminar sub-layer thickness [m]
δ_T thermal depth of ceiling layer in KYS model [m]
δ_U velocity depth of ceiling layer in KYS model [m]
ΔT temperature rise in fire plume [K]
ΔT_0 maximum temperature rise in fire plume [K]
ΔT_m maximum temperature rise in ceiling layer [K]
ΔT_{clng} temperature rise of the ceiling [K]
ΔT_{corr} temperature correction to account for ceiling heating [K]
ΔT^* normalized temperature rise in the turning region [-]
ΔT_m^* normalized maximum temperature rise in ceiling layer [-]
ΔT_{CL}^* normalized temperature rise in the ceiling layer [-]
ΔT_{FP}^* normalized temperature rise in the fire plume [-]
$\Delta T_{0,H}$ maximum temperature rise in the fire plume at the ceiling [K]
γ merging coefficient for profiles in the turning region [-]
η normalized radial distance from plume axis [-]
ρ gas density [kg/m^3]
$\Delta\rho$ gas density defect from ambient [kg/m^3]
ρ_∞ ambient gas density [kg/m^3]
ℓ_T thermal depth of ceiling layer in modified model [m]
$\ell_{T,tr}$ thermal depth of ceiling layer in modified model at the end of the turning region [m]
ℓ_U velocity depth of ceiling layer in modified model [m]

Subscripts

0 maximum value on plume axis
0,H maximum value on plume axis at the ceiling
c convective
ent enthalpy
CL ceiling layer
FP fire plume
T thermal layer
U velocity layer
tr turning region
lim transition from reacting to non-reacting plume region

Superscripts

* normalized quantity

References

1. G. Heskestad, "Fire Plumes, Flame Height, and Air Entrainment," in *The SFPE Handbook of Fire Protection Engineering*, 4th ed.: SFPE, 2008, ch. 1 sec. 2, pp. 2-1 to 2-17.

2. R. L. Alpert, "Ceiling Jet Flows," in *The SFPE Handbook of Fire Protection Engineering*, 4th ed.: SFPE, 2008, ch. 2 sec. 2, pp. 2-18 to 2-31.

3. F. Tamanini, "Heat Release Rate and Sprinkler Response Characterization in Large-Scale Fires," in *Proc. of the Sixth International Seminar on Fire and Explosion Hazards*, 2011, pp. 330-341.

4. H-C Kung, H-Z You, and R. D. Spaulding, "Ceiling Flows of Growing Rack Storage Fires," in *Twenty-First Symposium (International) on Combustion*, 1986, pp. 121-128.

5. B. J. McCaffrey, "Purely Buoyant Diffusion Flames," National Bureau of Standards, NBSIR 79-1910, October 1979.

6. W. K. George, R. L. Alpert, and F. Tamanini, "Turbulence Measurements in an Axisymmetric Buoyant Plume," *Int. J. Heat Mass Transfer*, vol. 20, pp. 1145-1154, 1977.

7. P. D. Beuther, S. P. Capp, and W. K. George, "Momentum and Temperature Balance Measurements in an Axisymmetric Turbulent Plume," *ASME Paper No. 79-HT-42*, 1979.

8. G. Heskestad, "Physical Modeling of Fire," *J. of Fire & Flammability*, vol. 6, p. 253, 1975.

9. R. L. Alpert, "Turbulent Ceiling-Jet Induced by Large-Scale Fires," *Comb. Sci. and Tech.*, vol. 11, p. 197, 1975.

10. G. Heskestad and T. Hamada, "Ceiling Jets of Strong Fire Plumes," *F. Safety J.*, vol. 21, p. 69, 1993.

11. X. Zhou, Private Communication, September 2015.

12. F. Tamanini, Unpublished Internal Document, February 2014.

Appendix A. Summary of Correlations for the Fire Plume, Ceiling Layer and Turning Region

A.1 Fire Plume

The fire plume equations are summarized here in simplified form[iii] by setting c_p = 1.0 kJ/kg K, g = 9.806 m/s^2, ρ_∞ = 1.19 kg/m^3, and T_∞ = 298K.

A.1.1 *Vertical Decay*

After substitution of 10.0 and 3.9 for 11.0 and 4.25, respectively in Eqs. 2-2 and 2-7 of the main body of this report, the simplified forms of the correlations introduced in Chapter 2 now become:

Flame region ($z < z_{lim}$)

$$\Delta T_0\left[K\right] = 3.5 \cdot T_\infty\left[K\right] \quad , \tag{A-1}$$

$$u_0\left[m/s\right] = 7.225 \cdot \left(\left(z - z_0\right)\left[m\right]\right)^{1/2} \quad . \tag{A-2}$$

Flame-plume transition region ($z = z_{lim}$)

$$\Delta T_{0,\lim}\left[K\right] = 3.5 \cdot T_\infty\left[K\right] \quad , \tag{A-3}$$

$$u_{0,\lim}\left[m/s\right] = 2.435 \cdot \left(\dot{Q}_c\left[kW\right]\right)^{1/5} \quad . \tag{A-4}$$

Plume region ($z > z_{lim}$)

$$\Delta T_0\left[K\right] = 0.09325 \cdot T_\infty \left(\dot{Q}_c\left[kW\right]\right)^{2/3} \left(\left(z - z_0\right)\left[m\right]\right)^{-5/3} \quad , \tag{A-5}$$

$$u_0\left[m/s\right] = 1.179\left(\dot{Q}_c\left[kW\right]\right)^{1/3} \left(\left(z - z_0\right)\left[m\right]\right)^{-1/3} \quad , \tag{A-6}$$

where z_{lim} is given by:

$$\left(z_{\lim} - z_0\right)\left[m\right] = 0.1136\left(\dot{Q}_c\left[kW\right]\right)^{2/5} \quad . \tag{A-7}$$

[iii] Since some of the numeric constants are not dimensionless, the corresponding equations require that parameters be entered in the indicated units. Where units are not specified, the equation is valid for any set of consistent units.

The location of the virtual origin is calculated from:

$$z_0[m] = z_{0,I}[m] + 0.095 \cdot \dot{Q}_c^{2/5}[kW] \quad , \qquad \text{A-8}$$

$$z_{0,I}[m] = -1.02 \cdot D[m] \qquad \text{for pool fires,} \qquad \text{A-9}$$

$$z_{0,I}[m] = -0.5\left[5 \cdot (n-1) + 4\right] \cdot 0.3048 \qquad \text{for rack storage of } n \text{ tiers.} \qquad \text{A-10}$$

A.1.2 *Radial Profiles*

The radial variation of temperature and vertical velocity in the fire plume is given by:

$$\Delta T = \Delta T_0 \exp(-0.6931\ (r/b_T)^2) \quad , \qquad \text{A-11}$$

and

$$u = u_0 \exp(-0.6931\ (r/b_U)^2) \quad , \qquad \text{A-12}$$

where the distance to the point where values are half of the centerline peak is:

$$b_U = 0.108 \cdot \left(1 + \frac{\Delta T_0}{T_\infty}\right)^{1/3} (z - z_0) \quad , \qquad \text{A-13}$$

and

$$b_T = 0.92 \cdot b_U \quad . \qquad \text{A-14}$$

A.2 Ceiling Layer

The correlations for the evolution of excess temperature and horizontal velocity in the ceiling layer are given by the following relationships.

A.2.1 *Horizontal Decay*

The radial evolution of peak excess temperature and velocity is:

$$\Delta T_m = \Delta T_{0,H} \left(\frac{r}{r_{tr}}\right)^{-2/3} \qquad \text{for } r/r_{tr} \geq 1 \ , \qquad \text{A-15}$$

and

$$u_m = u_{0,H} \left(\frac{r}{r_{tr}}\right)^{-4/5} \qquad \text{for } r/r_{tr} \geq 1 \ . \qquad \text{A-16}$$

where $\Delta T_{0,H}$ and $u_{0,H}$ are given by Eqs. A-1 or A-5 and A-2 or A-6, respectively, with H_0 replacing $z - z_0$.

In the above expressions, the inner radius of the ceiling layer is:

$$r_{tr} = 0.162 \cdot \left(1 + \frac{\Delta T_{0,H}}{T_\infty}\right)^{1/3} H_0 \qquad \text{for } z_{lim} \le H$$

$$r_{tr} = 0.162 \cdot \left(\frac{T_{0,H}}{T_\infty}\right)^{1/3} \left(H - z_0\right) + z_{\lim} - H \qquad \text{for } z_{lim} > H \quad . \qquad \text{A-17}$$

A.2.2 *Vertical Profiles*

The variation of peak excess temperature and velocity with distance from the ceiling is:

$$\Delta T = \Delta T_m \qquad \text{for } 0 < y < \delta$$

$$\Delta T = \Delta T_m \, \exp\left[-\left(\frac{y-\delta}{\ell_T}\right)^2\right] \qquad \text{for } y \ge \delta \quad , \qquad \text{A-18}$$

and

$$u = u_m \qquad \text{for } 0 < y < \delta$$

$$u = u_m \, \exp\left[-\left(\frac{y-\delta}{\ell_U}\right)^2\right] \qquad \text{for } y \ge \delta \quad , \qquad \text{A-19}$$

where y (= $H - z$) is distance down from the ceiling and

$$\delta[m] = 0.013 \cdot \{H_0[m]\}^{-1/3} \, r[m] \quad , \qquad \text{A-20}$$

$$\ell_T = 0.11 \cdot H_0 \cdot \left[1 + 1.5 \cdot \left(1 + \frac{\Delta T_{0,H}}{T_\infty}\right) \exp\left(-6.4 \frac{r}{H_0}\right)\right] \cdot \left[1 - \exp\left(-1.8 \cdot \frac{r}{H_0}\right)\right] \quad , \qquad \text{A-21}$$

$$\ell_U = 0.8 \cdot \ell_T \quad . \qquad \text{A-22}$$

In all the above equations, the presence of "H" in the subscript denotes a quantity at the ceiling ($z = H$) and H_0 has been used as shorthand notation for $H - z_0$.

A.3 Turning Region

In the turning region of the flow, which is approximately characterized by the domain $0 < r < r_{tr}$ and $0 < y < r_{tr}$, a smooth transition is enforced from the vertical fire plume to the horizontal ceiling layer.

A.3.1 *Excess Temperature*

For $r / r_{tr} \leq 1$, the inward extension of the temperature profile in the ceiling layer is assumed to be given by:

$$\Delta T_{CL} = \Delta T_{0,H} \qquad \text{for } 0 < y < \delta$$
$$\Delta T_{CL} = \Delta T_{0,H} \exp\left[-\left(\frac{y-\delta}{\ell_{T,tr} \cdot r_{tr}/r} \right)^2 \right] \qquad \text{for } y \geq \delta \quad , \tag{A-23}$$

while Eqs. A-15 and A-18 remain valid for $r/r_{tr} > 1$. The depth of the thermal layer at the transition radius, r_{tr}, is:

$$\ell_{T,tr} = 0.11 \cdot H_0 \cdot \left[1 + 1.5 \cdot \left(1 + \frac{\Delta T_{0,H}}{T_\infty} \right) \exp\left(-6.4 \frac{r_{tr}}{H_0} \right) \right] \cdot \left[1 - \exp\left(-1.8 \cdot \frac{r_{tr}}{H_0} \right) \right] \quad . \tag{A-24}$$

The excess temperature in the fire plume is given by:

$$\Delta T_{FP} = \Delta T_0 \exp\left[-0.6931 \left(\frac{r}{0.09936 \cdot (1 + \Delta T_0 / T_\infty)^{1/3} \cdot (H_0 - y)} \right)^2 \right] \quad , \tag{A-25}$$

where ΔT_0 is the peak temperature rise on the plume axis at distance y from the ceiling:

$$\Delta T_0 = \Delta T_{0,H} \left(1 - \frac{y}{H_0} \right)^{-5/3} \qquad \text{for } y \leq y_{lim}$$
$$\Delta T_0 = 3.5 \cdot T_\infty \qquad \text{for } y > y_{lim} \quad , \tag{A-26}$$

with

$$y_{\lim} = H_0 \left[1 - \left(\frac{1}{3.5} \frac{\Delta T_{0,H}}{T_\infty} \right)^{3/5} \right] \quad . \tag{A-27}$$

The merging of the two profiles for the fire plume and for the inward extrapolated ceiling layer is done by setting:

$$\Delta T = \Delta T_{FP} + \gamma \, \Delta T_{CL} \quad , \tag{A-28}$$

where

$$\gamma = 1 - \frac{\Delta T_{FP,0}}{\Delta T_{CL,0}} \exp\left(-\frac{r}{r_{tr}} \frac{y}{r_{tr}} \frac{\ell_{T,tr}}{\ell_T} \right) \quad . \tag{A-29}$$

In the above equation, the two quantities $\Delta T_{FP,0}$ and $\Delta T_{CL,0}$ refer to the values of ΔT_{FP} and ΔT_{CL} at radius, *r*, and at *y* = 0, i.e, at the ceiling.

A.3.2 *Scalar Velocity*

Similar formulas are used in the case of the scalar velocity field. In this case, the transition is approached by reference to the velocity magnitudes, neglecting the fact that the flow is vertical in the fire plume and horizontal in the ceiling layer. The orientation of the velocity vectors could conceivably be estimated, but is not attempted here.

For $r / r_{tr} \le 1$, the inward extension of the velocity profile in the ceiling layer is assumed to be given by:

$$\begin{aligned} u_{CL} &= u_{0,H} && \text{for } 0 < y < \delta \\ u_{CL} &= u_{0,H}\ \exp\left[-\left(\frac{y-\delta}{\ell_{U,tr}\cdot r_{tr}/r}\right)^2\right] && \text{for } y \ge \delta \quad , \end{aligned} \qquad \text{A-30}$$

while Eqs. A-16 and A-19 remain valid for $r/r_{tr} > 1$. The depth of the velocity layer at the transition radius, r_{tr}, is:

$$\ell_{U,tr} = 0.088\cdot H_0\cdot\left[1+1.5\cdot\left(1+\frac{\Delta T_{0,H}}{T_\infty}\right)\exp\left(-6.4\,\frac{r_{tr}}{H_0}\right)\right]\cdot\left[1-\exp\left(-1.8\cdot\frac{r_{tr}}{H_0}\right)\right] \quad . \qquad \text{A-31}$$

The velocity in the fire plume is given by:

$$u_{FP} = u_0\ \exp\left[-0.6931\left(\frac{r}{0.108\cdot(1+\Delta T_0/T_\infty)^{1/3}\cdot(H_0-y)}\right)^2\right] \quad , \qquad \text{A-32}$$

where u_0 is the peak velocity on the plume axis at distance *y* from the ceiling:

$$\begin{aligned} u_0 &= u_{0,H}\ \left(1-\frac{y}{H_0}\right)^{-1/3} && \text{for } y \le y_{lim} \\ u_0 &= u_{0,\lim}\ \left(\frac{1-y/H_0}{1-y_{\lim}/H_0}\right)^{1/2} && \text{for } y > y_{lim} \quad , \end{aligned} \qquad \text{A-33}$$

where y_{lim} is given by Eq. A-27 and $u_{0,lim}$ is calculated from the first of the two above equations by setting $y = y_{lim}$.

Similar to the case of the temperature profiles, the merging of the fire plume and the inward extrapolated ceiling layer is done by setting:

$$u = u_{FP} + \gamma\, u_{CL} \quad , \tag{A-34}$$

where

$$\gamma = 1 - \frac{u_{FP,0}}{u_{CL,0}} \exp\left(-\frac{r}{r_{tr}} \frac{y}{r_{tr}} \frac{\ell_{U,tr}}{\ell_U} \right) \quad . \tag{A-35}$$

In the above equation, the two quantities $u_{FP,0}$ and $u_{CL,0}$ refer to the values of u_{FP} and u_{CL} at the ceiling (i.e, at $y = 0$) and at radius, r.

Because of the rapid radial decay of the fire plume profiles, their contribution can be neglected for $r/r_{tr} > 2$-2.5. Also, the contribution from the ceiling layer values can be neglected at locations close to the axis, as defined by $r/r_{tr} \leq 0.01$. Therefore, the interpolation procedure only needs to be applied in the range $0.01 < r/r_{tr} < 2.5$.

Appendix B. Effect of Turbulence Fluctuations on Enthalpy and Mass Fluxes in Fire Plumes

This appendix provides an estimate of the effect of turbulence on estimates of the integrated vertical fluxes of enthalpy and mass in fire plumes.

B.1 Enthalpy Flux

As introduced by Eq. 2-17 in the main body of the report, the enthalpy flux in an axisymmetric fire plume is given by:

$$\dot{Q} = 2\pi \int_0^\infty c_p \, \Delta T \, \rho \, u \, r \, dr \qquad . \tag{B-1}$$

For the purposes of the present analysis, only the variables that are affected by turbulent fluctuations need to be retained. More specifically, Eq. B-1 applied to instantaneous values can be simplified to:

$$\dot{Q} \approx \Delta T \, \rho \, u \qquad . \tag{B-2}$$

where ΔT (= $T - T_\infty$), ρ and u represent temperature rise above ambient, gas density and vertical velocity.

By replacing instantaneous values with average (denoted by an overbar) and fluctuating (denoted by a prime) components, Eq. B-2 can be rewritten as:

$$\dot{Q} \approx \left(\Delta\overline{T} + T'\right)\left(\overline{\rho} + \rho'\right)\left(\overline{u} + u'\right) \qquad , \tag{B-3}$$

or, by introducing the equation of state:

$$\dot{Q} \approx \frac{\left(\Delta\overline{T} + T'\right)}{\left(\overline{T} + T'\right)}\left(\overline{u} + u'\right) \qquad . \tag{B-4}$$

After algebraic manipulation, time averaging and neglecting of higher-order terms, Eq. B-4 reduces to the following expression:

$$\overline{\dot{Q}} \approx \frac{\Delta\overline{T}}{\overline{T}}\overline{u}\left[1 + \frac{T_\infty}{\overline{T}}\frac{\overline{u'T'}}{\overline{u}\,\Delta\overline{T}}\right] \qquad . \tag{B-5}$$

The term in front of the square brackets represents the enthalpy flux that would be calculated on the basis of average quantities alone. The second term inside the square brackets is the contribution from turbulent fluctuations. This contribution can be expressed as:

$$\frac{T_\infty}{\overline{T}}\frac{\overline{u'T'}}{\overline{u}\,\Delta\overline{T}} = \frac{T_\infty}{\overline{T}}\,\frac{\overline{u'T'}}{\sqrt{\overline{u'^2}\,\overline{T'^2}}}\,\frac{\sqrt{\overline{u'^2}}}{\overline{u}}\,\frac{\sqrt{\overline{T'^2}}}{\Delta\overline{T}} \quad . \tag{B-6}$$

By substituting the values for the three correlations in the right-hand side of the equation with values reported in Ref. [6], the contribution from turbulent fluctuations becomes:

$$\frac{T_\infty}{\overline{T}}\frac{\overline{u'T'}}{\overline{u}\,\Delta\overline{T}} = 0.65\cdot 0.25\cdot 0.35\,\frac{T_\infty}{\overline{T}} = 0.057\,\frac{T_\infty}{\overline{T}} \quad . \tag{B-7}$$

or, in other words, the turbulent fluctuations contribute at most about 6% to the enthalpy flux calculated on the basis of average quantities alone. Owing to the term $T_\infty/\overline{T}$, the contribution becomes even lower, the higher the temperatures in the plume.

B.2 Mass Flux

In the case of the mass flux, the starting point is Eq. 2-30 in the main body of the report:

$$\dot{m} = 2\pi \int_0^\infty \rho\, u\, r\, dr \quad . \tag{B-8}$$

By following the same approach used with the enthalpy flux, the instantaneous mass flow can be written as:

$$\dot{m} \approx \rho u \quad , \tag{B-9}$$

or, by introducing the equation of state and writing instantaneous quantities using average and fluctuating components:

$$\dot{m} \approx \left(\overline{u} + u'\right)/\left(\overline{T} + T'\right) \quad . \tag{B-10}$$

After algebraic manipulation, time averaging and neglecting of higher-order terms, Eq. B-10 reduces to the following expression:

$$\overline{\dot{m}} \approx \frac{\overline{u}}{\overline{T}}\left[1 - \frac{\overline{u'T'}}{\overline{u}\,\overline{T}}\right] \quad . \tag{B-11}$$

The second term inside the square brackets representing the contribution from turbulent fluctuations can be written as:

$$\frac{\overline{u'T'}}{\overline{u}\,\overline{T}} = \frac{\Delta\overline{T}}{\overline{T}}\,\frac{\overline{u'T'}}{\sqrt{\overline{u'^2}\,\overline{T'^2}}}\,\frac{\sqrt{\overline{u'^2}}}{\overline{u}}\,\frac{\sqrt{\overline{T'^2}}}{\Delta\overline{T}} \cong 0.057\,\frac{\Delta\overline{T}}{\overline{T}} \quad . \tag{B-12}$$

In Eq. B-12, the same correlation values reported in Ref. [6] have been used to obtain the final equality. Because of the term $\Delta\overline{T}/\overline{T}$, the contribution from turbulent fluctuations to the mass flux in the non-reacting portion of the fire plume can be considered to amount only to a few percentage points and, even so, only in the case where the average temperature rise, $\Delta\overline{T}$, is of the same order as the absolute temperature, $\overline{T}$. In the limit of small temperature changes, the contribution to mass flux from turbulence fluctuations is negligible.

FM Insurance Company Limited
1 Windsor Dials, Windsor, Berkshire, SL4 1RS
Authorized by the Prudential Regulation Authority and regulated by the Financial Conduct Authority and the Prudential Regulation Authority.